

NICOLA SCHLATTER, BSc

**Modification of the
auroral E-region
with powerful HF waves**

MASTER THESIS

For obtaining the academic degree
Diplom-Ingenieur

Master Program of
Technical Physics



University of Technology Graz

Supervisor:

Ao.Univ-Prof. Dipl.-Ing. Dr.phil Martin Heyn

Institute of Theoretical and Computational Physics

Graz, November 2010

Acknowledgment

This master thesis was written at the Alfvén Laboratory at the Royal Institute of Technology in Stockholm. I would like to thank my supervisor at the Alfvén Laboratory Nikolay Ivchenko for introducing me to a fascinating field of research. I would also like to thank the team members of campaigns I took part. Namely these are Hanna Dahlgren, Björn Gustavsson, Vasyl Belyey, Dan Whiter, Urban Brändström and Brendan Goodbody.

Also I would like to thank my family for supporting me during my studies in Graz and Stockholm.

Abstract

Data from an ionospheric heating experiment in Tromsø have been analyzed. The experiment was carried out during auroral conditions in October 2006. Beside data from the EISCAT UHF radar also optical data were recorded with the ASK (auroral structure and kinetics) instrument and enhancements of backscattered power from the E-region were studied. Two simultaneous layers of instability with an altitude separation of ~ 5 km are observed at an altitude of ~ 120 km. The two layers differ in their spectral characteristics and show different time evolution. For one heating cycle it was also found that auroral processes correlate to the strength of enhancements and the characteristics of the ion line spectra.

Zusammenfassung

Die Daten eines ionospheric heating Experiments in Tromsø wurden ausgewertet. Zur Verfügung stehen Daten des EISCAT UHF incoherent scatter radars und des ASK (auroral structure and kinetics) optischen Instrumentes. Das Experiment wurde in 2006 gleichzeitig mit dem Auftreten von Nordlichtern durchgeführt, dabei wurden Verstärkungen im zurück gestreuten Radar Signal der UHF Anlage gemessen, welche auf die parametric decay instability zurück zuführen sind. In dieser Master of Science Arbeit wurden Verstärkungen aus dem Bereich der Ionosphärischen E-region untersucht. Es wurden zwei zur selben Zeit auftretende Schichten mit einem Höhen Unterschied von ~ 5 km gefunden. Die zwei Schichten unterscheiden sich in deren Characteristic der ion acoustic waves wobei die untere Schicht die Parametric Decay Instability und die obere die Oscillating Two Stream Instability als Verursacher nahelegt. Ausserdem wurde bei einem heating Zyklus Korrelation zwischen der Aktivität der Nordlichter und der Intensität der beobachteten Plasma Instabilität beobachtet.

Contents

Contents	7
1 Introduction	1
1.1 The Ionosphere	1
1.2 Aurora	2
1.3 Ionospheric heating	3
1.4 Incoherent scatter radar technique	4
2 Instrumentation	5
2.1 Heating facility	5
2.2 Incoherent Scatter Radar	6
2.3 ASK	7
3 Physics	9
3.1 Basic equations	9
3.2 Electromagnetic Waves in the Ionosphere	10
3.3 Electrostatic waves	15
3.4 Plasma Instability	18
4 Experiment and Data Overview	23
4.1 Radar Data and Software	23
4.2 Optical Data and Software	24
4.3 Overview of Data	24
5 PDI in the auroral E-region	33
5.1 Heating cycle O1	33
5.2 Heating cycle O2	40
5.3 Heating cycle O7	45
5.4 Heating cycle O8	50
5.5 Further Analysis	55
5.6 Summary of observations	55

6 Discussion	59
7 Conclusions	63
References	65
Bibliography	65

Chapter 1

Introduction

Underlying this master thesis report is an ionospheric heating experiment which was conducted on 20 October 2006. In such an experiment the interaction between powerful HF waves and the ionosphere is studied. In this first chapter a brief introduction into the nomenclature used is given followed by the instrumentation used. The second chapter will give an introduction to the physics involved and will be followed by a chapter giving an overview of the data and one for presenting analysis which was done.

1.1 The Ionosphere

The ionosphere is one part of Earth's atmosphere consisting of many different layers. Each of these layers can be described by their physical properties such as density or temperature. These physical properties can also describe different layer schemes. The atmosphere described in terms of temperature has different boundaries than when described by particle density. The ionosphere is the outermost part of the atmosphere - starting at about 85 km - and its distinctive feature is the high number of ions and electrons and on the other hand increasing temperature with altitude.

The ionosphere consists of species such as O, O₂ or N₂. Because of their different mass these species have different scale heights, i.e., the density of molecular oxygen is decreasing slower with increasing altitude than that of molecular oxygen. Ionization of the atmospheric species due to sunlight and cosmic radiation combined with the different scale heights lead to layering of the ionosphere. With the so called Chapman approach these layers can be approximated. In Figure 1.1 the four main regions are shown with altitude and electron density. The experiment underlying this thesis was carried out in the E-region which is located between 90 and 150 km. Above the E-region

is the F-region reaching altitudes to ~ 600 km.

As stated above the ionization happens because of sunlight and other sources of energy. Therefore the ionospheric structure also changes with time of day and season. For example, the E-layer disappears after sunset and the electron density drops from $\sim 2 \cdot 10^{11} \text{ m}^{-3}$ to $\sim 2 \cdot 10^9 \text{ m}^{-3}$, see Fälthammar [2001]. In Figure 1.2(a) a plot shows the number density of the different species in the E-layer. The underlying data are not from a measurement but are taken from the IRI model. The IRI model [IRI, 2010] takes into account daytime, year and of course the location and gives an estimate for the ion population in the ionosphere. In the E-Layer the density of neutrals is large compared to the density of ions. A different model of the atmosphere called MSIS-E-90 [MSIS, 2010] was used to estimate the neutral density. Because of the high neutral density in the E-layer and therefore high collision frequency (see Fig. 1.2(b)) results from experiments in the E-layer usually are different from those in layers higher up such as the F-layer.

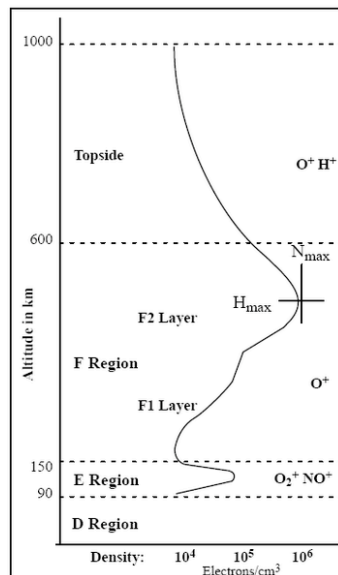


Figure 1.1: Electron density in the ionosphere dividing the ionosphere in different layers [Anderson and Fuller-Rowell, 2010].

1.2 Aurora

Aurorae are the result of energetic electrons hitting the atmosphere of the Earth. When these electrons reach altitudes with high densities they ionize

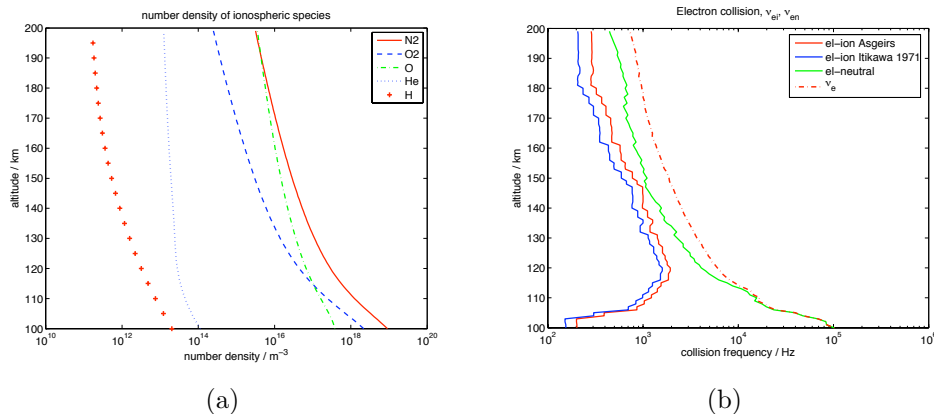


Figure 1.2: Important properties of the E-layer out of the IRI [IRI, 2010] and MSIS-E-90 [MSIS, 2010] model for Tromsø at 17:00 UT on the 20 October 2006.

- a) Showing the number density of species populating the E-layer.
 b) Collision frequency in the ionospheric E-layer.

neutral atoms and molecules. The emissions we see are a result of the relaxation processes in which an electron captured by an ion changes its energy level. During this processes photons are emitted with a certain energy corresponding to the species involved. A complete description of auroral processes and the coupling of the Earth-Sun system which plays a significant role is beyond the scope of this report (see e.g. Paschmann et al. [2003]). However auroral electrons disturb the ionospheric plasma and introduce irregularities therein. Also these electrons represent a second electron population beside the thermal electron population in the ionosphere.

1.3 Ionospheric heating

Ionospheric heating refers to experiments in which powerful HF waves are used to interact with the ionosphere. The name heating goes back to the fact that the coupling between a HF wave and plasma leads to heating of the electrons therein. Beside heating also plasma instabilities can be triggered. These possibilities make the ionosphere a huge laboratory for plasma experiments with the advantage of scale lengths which can not be realized in laboratory plasmas. Heating experiments have been conducted favoring the F-region of the ionosphere during quiet ionospheric conditions in order to have few irregularities. Therefore auroral conditions such as underlying the experiment

in this report are usually avoided.

1.4 Incoherent scatter radar technique

Incoherent scatter radars are powerful instruments to measure plasma properties in the ionosphere. The principle of measurement is to send a short radar pulse and measure the signal which is backscattered by the charged particles in the ionosphere. The technique of incoherent scatter radars was developed in the 1960s and many facilities exist around the world. Incoherent scatter radars contributed to the understanding of important processes in the Earth's ionosphere. Although the technique is being used for a long time many scientific problems remain unanswered and further research is needed. In order to provide observations with higher spatial and temporal resolution the technique is still being developed. A short introduction in the operational principle of incoherent scatter radars will be given in section 3.3

Chapter 2

Instrumentation

At the EISCAT (European Incoherent Scatter) Tromsø site several of different scientific instruments are placed. During the underlying experiment the EISCAT UHF radar, heating facility and the ASK instrument were operated. The site is placed 10 km south-east of Tromsø in the valley Ramfjorden at $69^{\circ}35'$ N latitude and $19^{\circ}14'$ E longitude. The site was originally built by the German Max-Planck-Institut für Aeronomie with the UHF radar between 1977-1980. Radar experiments and heating experiments in Tromsø have led to significant scientific results and a better understanding of ionospheric processes. Beside experiments of interest for plasma physicists also other experiments are conducted e.g. space debris or meteor observations.

2.1 Heating facility

The EISCAT heating facility was first built in 1979 and has since been upgraded and extended. Some of the main technical characteristics are given here. For a detailed description of the EISCAT Tromsø heater see the eiscat-heater webpage [Rietveld, 2010] where this information is taken from. Also a review on scientific results and problems investigated with this heater has been published, see Kohl et al. [1993]. The name heater for a powerful HF facility is because of the powerful HF wave interacts with the ionospheric plasma and this interaction can raise the electron temperature strongly.

The facility consists of transmitters, antennas and a control system. There are 12 power amplifiers each with 100 kW continuous rating. The frequency can be tuned from 3.58 to 8 MHz in principle, but only a few frequencies have been allocated. Therefore the lowest usable frequency is 4.04 MHz which is also the frequency used in this experiment.

The antennas consist of three arrays, but only two arrays cover the frequency of

4.04 MHz. The arrays each have 6×6 crossed dipole antennas each and an antenna gain of 23 dBi. Due to the antenna geometry the half power beamwidth is about 14° and the maximum effective radiated power is 300 MW.

Phase shifting, modulation of the heater beam, heater power and heating mode are controlled by a PC running a given scheme. The heater beam can also be tilted in the north-south plane by about $\pm 30^\circ$. To give an estimate of the electric field at a distance R the following equation can be used which is valid for free space:

$$E = \frac{\sqrt{(ERP(\text{kW}))}}{4R(\text{km})}, \quad (2.1)$$

where ERP is the effective radiated power by the antenna arrays and E the electric field strength. For an altitude of 120 km which corresponds to the E-layer altitude an electric field of 1.14 V/m for one array is estimated. This is only a rough estimation of the electric field. For a more precise estimation the absorption of wave energy below the altitude of interest has to be taken into account. Such an estimation of below E-layer absorption could be made by analyzing data of the ionosonde at the EISCAT site.

2.2 Incoherent Scatter Radar

As stated above the EISCAT site contains a VHF radar with a frequency of 225 MHz and a UHF radar at 930 MHz. The UHF has a parabolic dish which is steerable. During the experiment the UHF radar was used in field aligned (185.1° azimuth and 77.5° elevation) position.

The principle of an incoherent scatter radar is to send a strong and very short pulse of an electromagnetic wave and subsequently measure the backscattered signal. The backscattering process of the wave is called Thomson scattering. When an electromagnetic wave passes an electron the electron starts oscillating with the frequency of the wave and radiates a small portion of the absorbed energy at the same frequency. The same happens to the ions, but due to their high mass the energy radiated by the ions is negligible compared to the energy radiated by the electrons. The technique of incoherent scatter radars was developed in the 1960s and is very powerful to measure important plasma properties of the ionosphere and several observatories exist, e.g., Millstone Hill, Arecibo, Jicamarca and of course the EISCAT radars.

More detailed Information about the radar program used will follow in chapter 4.

2.3 ASK

ASK (auroral structure and kinetics) is an instrument developed by the Alfvén Laboratory at KTH and a group at the university of Southampton. It is a multi-spectral imager containing three EMCCD cameras providing high temporal and spatial resolutions. In Figure 2.1 an image taken with the ASK1 camera is shown. Each of the cameras is equipped with a narrow field of view lens with $3 \times 3^\circ$ FOV and interference filters. The interference filters pick up the wanted auroral emission line, the filters are listed in Table 2.1. Since different emissions have different life times (time between excitation and emission) the flow of the plasma can be monitored giving the name of the instrument. The three different imagers can also be used to monitor auroral emissions corresponding to different energies of the precipitating electrons. A description of the ASK instrument is given in the paper by Dahlgren et al. [2008].

Table 2.1: Used Filters for the three imagers of the ASK instrument during the October 2006 campaign showing the central wavelength, the full width at half maximum and the target emission.

	$\lambda_{cent} / \text{\AA}$	FWHM / \AA	emission
ASK1	6730	140	N ₂ 1PG; high energy
ASK2	7319	10	O ⁺ ; long-lived
ASK3	7774	15	O; low energy

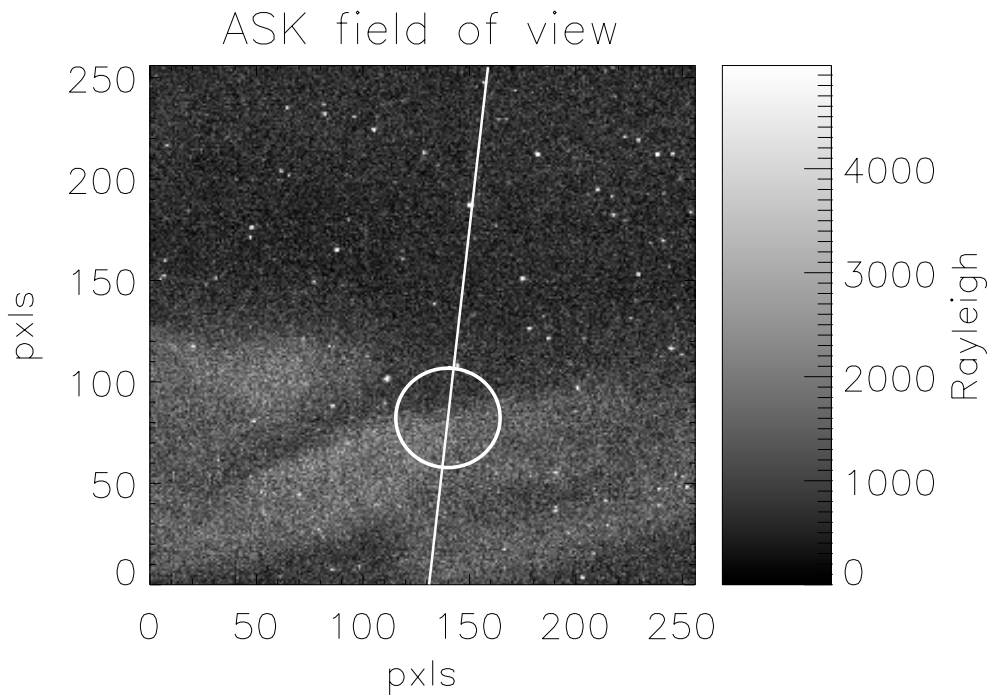


Figure 2.1: Image taken with the ASK1 imager during an auroral event at 18:12:33 on October 20 2006. The circle corresponds to the radar beam and the line indicates the north-south direction where north is at the bottom (east is to the right). The center of the circle in the image above is also the direction of magnetic zenith.

Chapter 3

Physics

3.1 Basic equations

The basic properties of a plasma can be described by three fundamental parameters which are given below. These parameters are determined by the density of the plasma species n_s , their temperature T_s and the magnetic field B .

A charged particle with a velocity component perpendicular to B spirals around the magnetic field due to the Lorentz force. The so called cyclotron frequency is given by

$$\omega_{cs} = \frac{q_s B}{m_s}, \quad (3.1)$$

where the index s stands for the species, q is the charge of the particle and m the particles mass. The second parameter is also a frequency and is called plasma frequency. It is an important timescale of the plasma and gives the frequency of, e.g., the electrons with which they oscillate around the positive charges if they would be displaced and then released. The plasma frequency is

$$\omega_{ps}^2 = \frac{n_s q_s^2}{\epsilon_0 m_s} \quad (3.2)$$

is independent of the magnetic field B , ϵ_0 is the dielectric constant and n_s the number density of the species s . The third parameter is called Debye length and is the characteristic length scale of the plasma. If we assume a positive charge put into the plasma the negative particles, i.e., the electrons would be attracted by this charge and shield the electric field of the positive space charge. The according length scale of the shielded electric field is the Debye length and is defined by

$$\lambda_D^2 = \frac{\epsilon_0 k T_e}{n_0 e^2} \quad (3.3)$$

where κ is the Boltzmann constant, e the electron charge, n_0 the electron density and T_e the electron temperature.

3.2 Electromagnetic Waves in the Ionosphere

The basic equations describing the coupling between the electric and magnetic field are Maxwell's equations. In order to analyze waves in plasma one has to couple the equation of motion for the particles in the plasma to Maxwell's equations. Maxwell's equations are

$$\nabla \times \mathbf{B} = \mu_0 \mathbf{J} + \epsilon_0 \mu_0 \frac{\partial \mathbf{E}}{\partial t} \quad (3.4)$$

$$\nabla \times \mathbf{E} = -\frac{\partial \mathbf{B}}{\partial t} \quad (3.5)$$

$$\nabla \cdot \mathbf{E} = \frac{\rho_q}{\epsilon_0} \quad (3.6)$$

$$\nabla \cdot \mathbf{B} = 0. \quad (3.7)$$

To model ionospheric conditions we assume a plasma with an external magnetic field. To simplify the equations we also assume the plasma to be cold which means there is no thermal motion. A commonly used procedure to derive the dispersion relation is to linearize the set of equations and transform them to Fourier space. The book by Gurnett and Bhattacharjee [2005] follows this approach, we will follow their chapter 4.4.

The force acting on the particles is the Lorentz force and in the case of waves in a uniform magnetized plasma the magnetic field is $\mathbf{B} = \mathbf{B}_0 + \mathbf{B}_1$, where \mathbf{B}_0 is the background magnetic field and \mathbf{B}_1 the wave field. The linearized particle equation of motion then reads as:

$$m_s \frac{\partial \mathbf{v}_s}{\partial t} = e_s [\mathbf{E} + \mathbf{v}_s \times \mathbf{B}_0], \quad (3.8)$$

where m_s is the particle mass and e_s the particle charge. The index s stands for the species, the index 0 for zero-order property and the term $\mathbf{v}_{s1} \times \mathbf{B}_1$ has been dropped due to linearization. For further simplification and without loss of generality we choose the magnetic field to be in z -direction. At this point we also transform the above equation to Fourier space and eqn. (3.8) in vector notation becomes:

$$\begin{aligned} -i\omega m_s \tilde{v}_{sx} &= e_s [\tilde{E}_x + \tilde{v}_{sy} B_0], \\ -i\omega m_s \tilde{v}_{sy} &= e_s [\tilde{E}_y + \tilde{v}_{sx} B_0], \\ -i\omega m_s \tilde{v}_{sy} &= e_s \tilde{E}_y. \end{aligned} \quad (3.9)$$

The \sim symbol above variables signifies that these are in Fourier space. With the above equation the current which is defined by $\tilde{\mathbf{J}} = \sum_s n_{s0} e_s \tilde{\mathbf{v}}$ can be computed and further the conductivity tensor σ defined by $\tilde{\mathbf{J}} = \sigma \cdot \tilde{\mathbf{E}}$. The conductivity tensor is then given by:

$$\sigma = \sum_s \frac{n_{s0} e_s^2}{m_s} \begin{bmatrix} \frac{-i\omega}{\omega_{cs}^2 - \omega^2} & \frac{\omega_{cs}}{\omega_{cs}^2 - \omega^2} & 0 \\ \frac{-\omega_{cs}}{\omega_{cs}^2 - \omega^2} & \frac{i\omega}{\omega_{cs}^2 - \omega^2} & 0 \\ 0 & 0 & \frac{i}{\omega} \end{bmatrix}. \quad (3.10)$$

The dielectric tensor which couples the electric field to the displacement current is given by $\mathbf{K} = \mathbf{1} - \frac{\sigma}{i\omega\epsilon_0}$ and has the form:

$$\mathbf{K} = \begin{bmatrix} S & -iD & 0 \\ iD & S & 0 \\ 0 & 0 & P \end{bmatrix}, \quad (3.11)$$

where

$$S = 1 - \sum_s \frac{\omega_{ps}^2}{\omega^2 - \omega_{cs}^2}, \quad D = \sum_s \frac{\omega_{ps}^2 \omega_{cs}}{\omega(\omega^2 - \omega_{cs}^2)} \quad (3.12)$$

and

$$P = 1 - \sum_s \frac{\omega_{ps}^2}{\omega^2} \quad (3.13)$$

In order to compute the dispersion relation we have to go back and take a look at Maxwell's equations. We can use Faraday's and Ampere's law to eliminate either \mathbf{E} or \mathbf{B} . In Fourier space the equations are:

$$\begin{aligned} i\mathbf{k} \times k\tilde{\mathbf{E}} &= -(-i\omega)\tilde{\mathbf{B}} \\ i\mathbf{k} \times \tilde{\mathbf{B}} &= -\frac{i\omega}{c^2}\mathbf{K} \cdot \tilde{\mathbf{E}}. \end{aligned} \quad (3.14)$$

Choosing to eliminate the magnetic field $\tilde{\mathbf{B}}$ we obtain a homogeneous equation for the electric field $\tilde{\mathbf{E}}$:

$$\mathbf{k} \times (\mathbf{k} \times \tilde{\mathbf{E}}) + \frac{\omega^2}{c^2}\mathbf{K} \cdot \tilde{\mathbf{E}} = 0. \quad (3.15)$$

The definition of the refractive index is $\mathbf{n} = c\mathbf{k}/\omega$ which we can use to simplify the equation above to:

$$\mathbf{n} \times (\mathbf{n} \times \tilde{\mathbf{E}}) + \mathbf{K} \cdot \tilde{\mathbf{E}} = 0. \quad (3.16)$$

We choose the coordinate system such that \mathbf{k} and therefore also \mathbf{n} lie in the x-z plane, remember \mathbf{B}_0 is along the z axis. The angle between \mathbf{B}_0 and \mathbf{n} is θ and we can write the refractive index \mathbf{n} :

$$\mathbf{n} = (n \sin \theta, 0, n \cos \theta). \quad (3.17)$$

Combined with the results from above for S , D and P we get the matrix equation:

$$\begin{bmatrix} S - n^2 \cos^2 \theta & -iD & n^2 \sin \theta \cos \theta \\ iD & S - n^2 & 0 \\ n^2 \sin \theta \cos \theta & 0 & P - n^2 \sin^2 \theta \end{bmatrix} \begin{bmatrix} \tilde{E}_x \\ \tilde{E}_y \\ \tilde{E}_z \end{bmatrix} = 0. \quad (3.18)$$

Non-trivial solutions to this equation can be found by computing the determinant of the matrix and setting it to zero which can be written as:

$$\tan^2 \theta = -\frac{P(n^2 - R)(n^2 - L)}{(Sn^2 - RL)(n^2 - P)}. \quad (3.19)$$

We will discuss in the following the case of waves traveling parallel to the magnetic field ($\theta = 0$) and the case of transverse traveling waves ($\theta = \pi/2$). Since the waves produced by the heater are traveling parallel to the magnetic field - in the beginning - we will start with this case.

Propagation parallel to the magnetic field

For waves parallel to the magnetic field we set $\theta = 0$ and the matrix equation (3.18) simplifies to:

$$\begin{bmatrix} S - n^2 & -iD & 0 \\ iD & S - n^2 & 0 \\ 0 & 0 & P \end{bmatrix} \begin{bmatrix} \tilde{E}_x \\ \tilde{E}_y \\ \tilde{E}_z \end{bmatrix} = 0. \quad (3.20)$$

The three non-trivial solutions are:

$$P = 0, \quad \tilde{\mathbf{E}} = (0, 0, E_0) \quad (3.21)$$

$$n^2 = R, \quad \tilde{\mathbf{E}} = (E_0, iE_0, 0) \quad (3.22)$$

$$n^2 = L, \quad \tilde{\mathbf{E}} = (E_0, -iE_0, 0), \quad (3.23)$$

where

$$R = 1 - \sum_s \frac{\omega_{ps}^2}{\omega(\omega + \omega_{cs})} \quad \text{and} \quad L = 1 - \sum_s \frac{\omega_{ps}^2}{\omega(\omega - \omega_{cs})}. \quad (3.24)$$

The first solution with $P = 0$ is associated with electrostatic oscillation with the frequency ω_p since the $\mathbf{v} \times \mathbf{B}$ force vanishes.

The second and the third root with $n^2 = R$ and $n^2 = L$ are transverse waves since the electric field is perpendicular to the wave vector \mathbf{k} . Also note the similarity to the dispersion relationship of warm plasma (see eqn. (3.27)) which

is discussed in section 3.3. With the use of Gauss's law it can be shown that there are no charge fluctuations associated with these waves and with Faraday's law it is easily shown that these waves are electromagnetic waves since the wave magnetic field is non-zero. The only difference between these two modes is that one is a right hand polarized wave and the other a left hand polarized which makes a huge difference in terms of wave plasma interactions. Electrons have a right-handed movement around the magnetic field while ions have a left-handed rotation. Therefore L-mode waves close to w_{ci} interact strongly with the ions whereas R-mode waves with a frequency close to the electron cyclotron frequency interact strongly with the electrons.

Those frequencies where the index of refraction is zero are called cut-off frequencies. At frequencies above the cut-off frequency the index of refraction is imaginary. In such regimes the wave is evanescent.

Propagation perpendicular to the magnetic field

As described above the dispersion relation for electromagnetic waves traveling parallel to the magnetic field has a cut-off which is close to the plasma frequency. In the ionosphere the electron density changes with altitude. Hence the heating wave can reach altitudes which are forbidden for waves traveling parallel to the magnetic field. What happens is that due to the changing refractive index with electron density the path of the wave is bent. Furthermore the wave can be reflected and at the reflection altitude the wave is directed perpendicular to the geomagnetic field.

Propagation perpendicular to the magnetic field corresponds to the case that $\theta = \pi/2$ and out of the dispersion relation and eqn. (3.18) we get two roots with their corresponding eigenvectors:

$$n^2 = P, \quad \tilde{\mathbf{E}} = (0, 0, E_0) \quad (3.25)$$

$$n^2 = \frac{RL}{S}, \quad \tilde{\mathbf{E}} = \left(\frac{iD}{S} E_0, E_0, 0 \right). \quad (3.26)$$

In the first case the magnetic field has no effect since the particle motion is parallel to the magnetic field and this mode is usually called ordinary (O) mode. The second solution is a bit more complicated since the wave interacts with the external magnetic field and this mode is therefore called extraordinary (X) mode. The fact that a heating wave is being slowed down close the reflection height and that the wave is linearly polarized in the case of an O-mode wave leads to swelling of the wave. The wave electric field at the so called

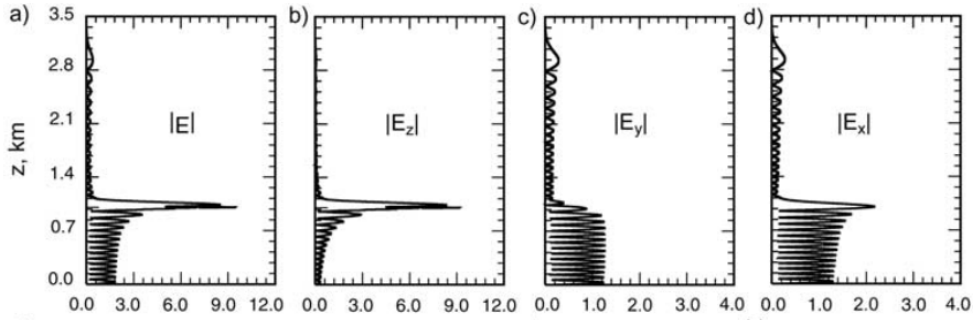


Figure 3.1: Figure taken from Gondarenko et al. [2003] (their Fig. 3) showing the effect of swelling for parameters of the Tromsø E-region. Plotted are the total electric field $|E|$ and the three components.

Airy maxima close to reflection can exceed the wave field by several times depending on the density gradient (Lundborg and Thide [1986], Shoucri et al. [1984]). Therefore the O-mode wave is privileged to excite plasma instabilities.

Depending on the shape of the electron density and the peak density it can also happen that parts of the heater wave tunnel through a thin density barrier or convert to an other mode and continue traveling upwards. An example for the study of so called mode conversion is the paper by Gondarenko et al. [2003] in which an example of mode conversion for parabolic density profiles above Tromsø is given. For this processes the angle of incidence of the wave on the ionosphere is of importance.

Ray paths

The half power beamwidth of the Tromsø heater is about 14° which leads to significantly different ray paths. Figure 3.2 [Leyser and Nordblad, 2009] summarizes important ray paths. The solid horizontal line marks the altitude where $\omega = \omega_p$ which is also called critical height. As a dashed line the upper hybrid height is shown. Three different types of ray-paths for an O-mode wave are seen. Bent paths to the right correspond to waves which are reflected at or close to the critical height. At the reflection altitude the k-vector of the wave is perpendicular to the magnetic field. The path in the middle shows an O-mode wave which converts to a X-mode wave which is called Z-mode in this context. The angles of incidence for the two paths to the right were chosen to be higher than the critical angle and end up in a so called Spitze region.

The ray paths in the Figure shown were calculated for a plane stratified density

profile. For a density profile containing irregularities, as it does during aurorae, the conversion from O-mode to Z-mode is not limited to one region. In such a case the conversion can happen also in the field-aligned direction.

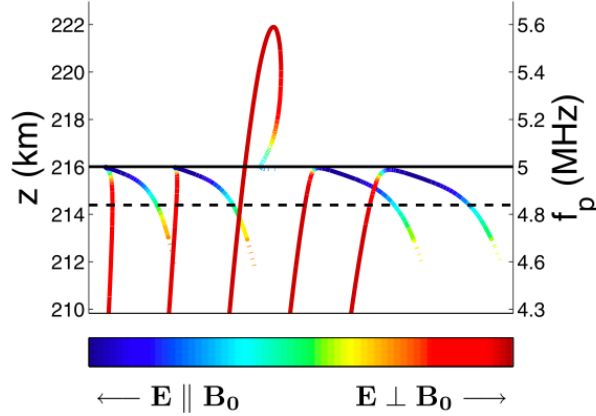


Figure 3.2: Different ray-paths from Leyser and Nordblad [2009]. The solid black line shows the critical height.

3.3 Electrostatic waves

In a plasma there are always waves present, e.g., thermally excited waves. In incoherent scatter radar experiments ion acoustic waves play a significant role. By measuring the spectra of these waves important plasma properties can be deduced such as the electron temperature. For this thesis we will limit this section to ion acoustic waves and Langmuir waves.

In order to describe a plasma with a non zero temperature a statistical approach is needed which is called kinetic theory.

Ion acoustic waves: To derive the dispersion relation for ion acoustic waves we will follow the approach of Gurnett and Bhattacharjee [2005] in their section 5. Out of a set of equations called the momentum equations and the adiabatic equation of state for a plasma the dispersion relation for ion and electron pressure waves can be derived. The roots of the dispersion relation can be separated into a transverse electromagnetic part and a longitudinal electrostatic part. The longitudinal part is:

$$D_l(k, \omega) = 1 - \sum_s \frac{\omega_{ps}^2}{\omega^2 - \gamma_s C_s^2 k^2} = 0, \quad (3.27)$$

where C_s is the acoustic speed and γ_s the adiabatic constant of the species s . Since the sum is over all species s one root exists for each species of the plasma. The root associated with electrons is called Langmuir mode and the one for ions the ion acoustic mode. Also compare eqn. (3.27) to the solutions found for electron oscillations in cold plasmas (eqn. 3.24 in section 3.2). We derive the dispersion relation for the ion acoustic mode with a significant simplification and assume that the ion temperature is small, i.e., $C_i = 0$:

$$1 - \frac{\omega_{pi}^2}{\omega^2} - \frac{\omega_{pe}^2}{\omega^2 - \gamma_e C_e^2 k^2} = 0. \quad (3.28)$$

Furthermore we assume that the phase velocity will be less than the electron thermal velocity $\omega^2 \ll \gamma_e C_e^2 k^2$ and get:

$$\omega^2 = \frac{1}{1 + \gamma_e \lambda_{De}^2 k^2} \left(\frac{\gamma_e \kappa T_e}{m_i} \right) k^2, \quad (3.29)$$

which is plotted in Figure 3.3(a). For long wavelengths i.e. $k\lambda_{De} \ll 1$ (in the case of the E-region and EISCAT UHF radar: $k = 30 \text{ m}^{-1}$ and $\lambda_{De} = 0.004 \text{ m}$ follows $k\lambda_{De} = 0.12$) we can simplify the above equation to:

$$\omega = \pm k \sqrt{\frac{\gamma_e \kappa T_e}{m_i}}. \quad (3.30)$$

In this approach we assumed the ion temperature to be much smaller than the electron temperature. To account for non zero ion temperatures the equal sign in the above equation has to be replaced by a proportional sign.

With the so called Landau approach it can be shown that the damping of ion acoustic waves is proportional to the square-root of T_i/T_e .

Langmuir waves: For completeness and due to the reason that Langmuir waves are important for the Parametric Decay Instability (see section 3.4) the dispersion relation will be given here. Starting from eqn. (3.27) we note that the mobility of the electrons is much higher than the mobility of the ions. Therefore we simplify eqn. (3.27) to:

$$1 - \frac{\omega_{pe}^2}{\omega^2 - \gamma_e C_e^2 k^2} = 0. \quad (3.31)$$

Rewriting the equation in terms of ω and using the relation $\omega_{pe}\lambda_{De} = C_e$ leads to:

$$\omega^2 = \omega_{pe}^2 \left(1 + \gamma_e \lambda_{De}^2 k^2 \right), \quad (3.32)$$

which is the dispersion relationship of the Langmuir mode and is plotted in Figure 3.3(b).

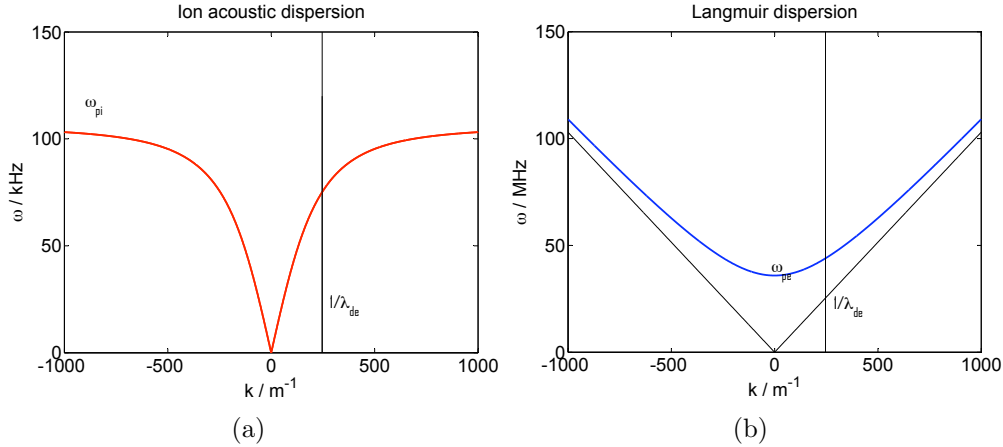


Figure 3.3: Dispersion relationship for the ion acoustic mode (a) and the Langmuir mode shown in (b). Also shown in (b) is the short wavelength approximation $\omega \sim k \sqrt{\frac{\gamma_e \kappa T_e}{m_e}}$. Both dispersion relations are plotted for values of the Tromsø E-region.

Incoherent Scatter Radar

A brief introduction to this technique will be given here. A short and powerful pulse of an electromagnetic wave ($\sim 10^8$ Hz) is sent towards the ionosphere where the wave is incident on the species therein. Most of the wave energy will pass the ionosphere however a small part will be scattered by a process which is called Thomson-scattering. Thomson-scattering describes the process of a wave incident on a charged particle. Due to the electromagnetic field the charged particle will start oscillating with the frequency of the wave. The oscillating charged particles will then radiate an electromagnetic wave which can be measured back on earth. Since ions are much heavier than electrons Thomson-scattering is more efficient for electrons.

The signal of the backscattered power includes information about plasma properties and is described in the following. The strength of the signal contains information about the number of electrons in the backscattering volume.

Electrons and ions usually have thermal distribution of their velocities and therefore each particle adds a different Doppler-shift to the backscattered signal leading to spectra of the backscattered signal which contain the ion temperature. Also waves in the ionosphere such as an ion-acoustic wave add a Doppler-shift leading to spectra. Since thermally excited ion acoustic waves always exist with up- and downward direction the resulting spectra are symmetric and called double hump spectra. An example of such a spectrum is shown in Figure 3.4. The same way as ion acoustic waves are detected by in-

coherent scatter radars also Langmuir waves can be detected. The frequency of Langmuir waves in the ionosphere is typically much higher than the one of ion acoustic wave which is in the order of kHz. In order to receive Langmuir waves and ion acoustic waves the incoherent scatter radar has to be operated in a special mode which was not done during the experiment studied in this report.

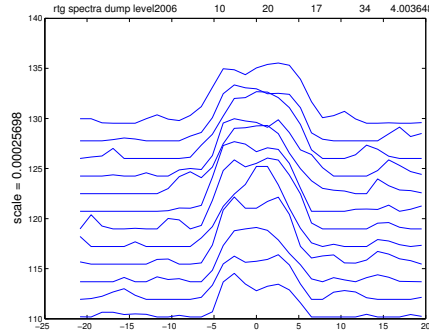


Figure 3.4: Typical observed spectra with the incoherent scatter technique. Shown are the spectra between 110 and 130 km altitude with amplitude (ordinate) vs. frequency (abscissa) averaged over one dump.

3.4 Plasma Instability

It has been already stated that a powerful HF wave incident on the ionosphere beside heating can also trigger plasma instabilities. One possibility of such an instability is the Parametric Decay Instability (PDI). A brief introduction into the important Parametric Decay Instability is given in the following.

Parametric Decay Instability

An electromagnetic wave incident on the ionospheric plasma can decay into other waves. For example a heater wave can decay into an ion acoustic wave and a Langmuir wave which is the case of PDI. This section follows the treatment of PDI in the paper "Introduction to ionospheric heating experiments at Tromsø - II" by Kohl et al. [1993].

We assume an electromagnetic wave incident on the ionosphere. This wave is in our case the pump wave or heater wave (ω_0, k_0) at which frequency the electrons will oscillate, the velocity of the oscillation is given by $v(z, t) \sim E_0 \cdot \cos(\omega_0 t - k_0 z)$. The density profile of the ionospheric plasma usually is

not completely smooth and perturbations in the electron density are always present. We assume these perturbations to be thermally excited perturbations which we describe as ion acoustic waves and are present in the ionosphere as seen, e.g., with the incoherent radar technique in the typical double hump spectra, see section 3.3. The background density N is superimposed by this density perturbations $n(z, t) = n_2 \cdot \cos(\omega_2 t - k_2 z)$. The current induced by the pump wave is then given by:

$$\begin{aligned} j &= (N + n) e v \sim (N + n) e \cdot E_0 \cos(\omega_0 t - k_0 z) \\ &= e N E_0 \cos(\omega_0 t - k_0 z) + n_2 (E_0/2) \cdot \{ \cos[(\omega_0 - \omega_2) t - (k_0 - k_2) z] \\ &\quad + \cos[(\omega_0 + \omega_2) t - (k_0 + k_2) z] \}. \end{aligned} \quad (3.33)$$

As seen in eqn.(3.33) beside the term with the original frequency ω_0 there is one wave with a higher and one with a lower frequency:

$$\begin{aligned} \omega_1 &= \omega_0 - \omega_2, \quad k_1 = k_0 - k_2 \\ \omega_3 &= \omega_0 + \omega_2, \quad k_3 = k_0 + k_2. \end{aligned} \quad (3.34)$$

The wavelength of the heater wave is of the order of hundred meters which is compared to the other considered waves much longer. Therefore we assume $k_0 \approx 0$. Due to the currents associated with the two waves two electric fields E_1 and E_3 are present which cause the electrons to oscillate with the frequency and wave number of $(\omega_1, -k_2)$ and (ω_3, k_2) . These waves are Langmuir waves, see section 3.3. One can see that these two waves are directed opposite to each other. We started assuming an ion acoustic wave with positive k-vector in z-direction since there are always up- and downward directed ion acoustic waves present there are also always resulting waves in both directions.

The Langmuir waves themselves couple to the pump wave and introduce a force on electrons which leads to density perturbations with the same frequency and wavevector as the originally assumed ion-acoustic waves [Kuo, 2003]. For this we note that in the hydrodynamic equation of motion for the electrons a nonlinear term appears

$$\rho \cdot \frac{\partial v}{\partial t} + \rho v \frac{\partial v}{\partial z} = -N e [E_0 \cos(\omega_0 t) + E_1 \cos(\omega_1 t - k_1 z)], \quad (3.35)$$

where $v = v(z, t)$ is the average electron velocity of the electrons in the volume element at altitude z and time t . We can calculate a first order velocity neglecting the nonlinear term $\rho v \frac{\partial v}{\partial z}$:

$$v_1 = -\frac{e}{m \omega_0} [E_0 \sin(\omega_0 t) + E_1 \sin(\omega_1 t - k_1 z)]. \quad (3.36)$$

Where $\omega_0 \approx \omega_1$ was used for simplicity. With this result we can estimate the nonlinear term in eqn.(3.35) and put the first order estimation v_1 into eqn.(3.35):

$$v_1 \frac{\partial v_1}{\partial z} = -\frac{e^2 k_1}{m^2 \omega_0^2} [E_0 E_1 \sin(\omega_0 t) \cos(\omega_1 t - k_1 z) + E_1^2 \sin(\omega_1 t - k_1 z) \cos(\omega_1 t - k_1 z)]. \quad (3.37)$$

Rearranging the terms using trigonometric identities leads to:

$$v_1 \frac{\partial v_1}{\partial z} = -\frac{k_1 e^2}{2m^2 \omega_0^2} \{E_0 E_1 \sin[(\omega_0 - \omega_1)t + k_1 z] + E_1^2 \sin[(\omega_1 - \omega_1)t + (k_1 - k_1)z]\} + \text{other terms.} \quad (3.38)$$

The other terms are high frequency terms in which we are not interested. The equation of motion for the electrons then reads as:

$$\rho \frac{\partial v}{\partial t} = -Ne [E_0 \cos(\omega_0 t) + E_1 \cos(\omega_1 t - k_1 z)] + \rho \frac{k_1 e^2}{2m^2 \omega_0^2} [E_0 E_1 \sin(\omega_2 t - k_2 z) + E_1^2]. \quad (3.39)$$

The second term on the right hand side appears to be of the frequency ω_2 which is the same frequency as the initial ion acoustic wave. The force represented by this term is called ponderomotive force. It also contains a term of frequency 0. This term is associated with the so called purely growing mode or oscillating two stream instability (OTSI).

In order to trigger the instability the heater electric field has to be above the threshold field E_{thr} since the amount of energy feed into the instability has to be higher than the losses due to damping. Fejer [1979] and others showed, that the three waves ω_1 , ω_2 and ω_3 may form a positive feedback circuit and the wave amplitudes grow exponentially if the pump wave field is above E_{thr} . The conditions for the growth can be formulated as: If the electric field of the Langmuir wave overcomes the threshold for the instability it can itself act as a pump wave. This cascade is limited by the fact that the pump power is limited and energy is dissipated, we will come back to this in the next paragraph. Another factor of limiting the growth of the wave amplitudes is that the dispersion relations for the ion acoustic and the Langmuir waves - derived in section 3.3 - have to be fulfilled approximately:

$$\omega_1^2 = \omega_p^2 (1 + 3k_1^2 \lambda_d^2) \quad (3.40)$$

$$\omega_2 = k_2 \sqrt{\frac{T_e \gamma_e \kappa}{m_i}}. \quad (3.41)$$

Therefore the daughter waves with the frequency ω_1 and ω_3 can not satisfy the dispersion relation both [Kuo, 2003]. In Figure 3.5(b) the resulting frequency lines are shown with indication of the amplitudes and in Figure 3.5(a) the conditions for PDI are illustrated showing the dispersion relation of the different waves and the matching condition, these Figures are taken from Kohl et al. 1993.

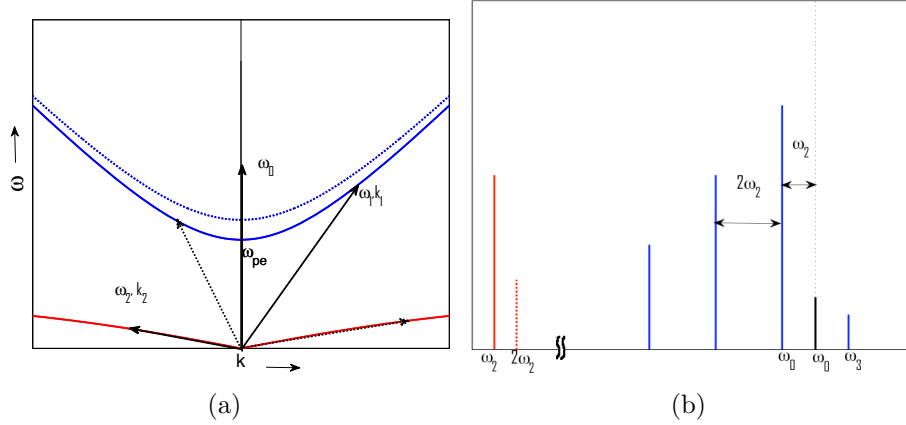


Figure 3.5: Figures after Kohl et al. [1993]. (a) shows the graphical solution of the PDI. The red line shows the ion-acoustic dispersion relation and the two blue lines the dispersion relation for the Langmuir mode for two different plasma frequencies. The black vectors show a graphical solution of the PDI. Dotted vectors correspond to a second decay. (b) summarizes the resulting frequency lines with the height indicating the amplitude of the resulting waves.

Threshold, Growth Rate

Different mathematical solutions have been presented describing parts of the observed turbulence characteristics. Some of the mathematical models are based on the so called Zakharov equations others on the fluid equation. These models lead to different predictions and not all describe the observed features with the same precision. Two important models are the Strong Langmuir turbulence (SLT) and the weak Langmuir turbulence (WLT) which are discussed in the paper by [Dubois et al., 1993]. A complete review of available models is not known by the author. Beside different mathematical concepts the difference between SLT and WLT is the limiting factor for the decay of the generated Langmuir waves. In the case of WLT the generated Langmuir waves "do not grow to sufficient field strengths to excite further waves" [Stubbe

et al., 1992] and in the case of SLT the generated and decayed Langmuir waves "have reached a frequency so close to ω_p that a decay to still lower frequencies becomes energetically impossible" [Stubbe et al., 1992].

Cascade, Matching height and OTSI

As described above the triggered Langmuir waves can reach field strengths above the threshold field. Therefore the Langmuir wave with the frequency ω_1 can trigger a second (cascade) wave with the frequency $\omega_1 - 2\omega_2$. This cascade process is also shown in Figure 3.5 indicated by the dashed lines.

In order to detect waves with a wave vector k_{wave} with the incoherent scatter radar the following equation has to be fulfilled:

$$k_{wave} = 2k_{radar}. \quad (3.42)$$

The altitude where this equation is fulfilled is called matching height and is the altitude at which Langmuir waves will be detected. For the EISCAT UHF system this altitude is usually several kilometers below the reflection altitude. In the derivation of the equation of motion for the electrons above a term associated with the OTSI appeared. The OTSI is a special case of the PDI where the frequency of the Langmuir mode is the heater frequency and the counterpart is a stationary density perturbation. According to Dubois et al. [1993] this instability is preferably triggered close to the reflection altitude.

Chapter 4

Experiment and Data Overview

Heating experiments have been done the last four decades and during this time many different experiments leading to a better understanding of plasma physics and ionospheric processes have been conducted. Reviews of heating experiments are given by Leyser and Wong [2009] and Kohl et al. [1993]. Although heating experiments have a long history not many experiments in the E-region and especially not during auroral conditions have been made. The underlying experiment was carried out at the EISCAT Tromsø site. In chapter 2 the instruments at the EISCAT site were introduced. For the heating experiment the heating facility was operated at 4.04 MHz which is the lowest possible frequency to operate. More details on heating mode and on/off times is given below.

4.1 Radar Data and Software

Beside own designed radar experiments also a set of radar programs which are ready for use exist. For the underlying data set the `arc1` program was used. This is a radar experiment using alternating codes for a higher range resolution. The decoded data consists of dumps of length 4 s with each containing 9 slices. One slice contains raw data for altitudes between 96 km and 422 km. Altitude resolution of the raw data is 0.9 km and the time resolution is 0.44 s. To process the raw data common programs exist like `guisdap` [Lehtinen et al., 1996] and `RTG`, where `RTG` is a program to monitor a radar experiment. `Guisdap` can be used to analyze raw data and obtain important plasma properties as electron density, electron temperature, ion velocity and the ratio of electron and ion temperature. In order to get useful estimates of this properties usually time and altitude integration of the raw data is necessary. For the `arc1` radar program useful time integration is one dump (4 s) minimum and

altitude integration which is dependent on the altitude. For E-region data no altitude integration is needed whereas in the F-region altitude integration over several altitude bins (~ 10 km) is useful due to the reduced signal strength from higher altitudes. All these processing parameters can be set using the `guidap` software package.

For ion line spectra the `RTG` package was used to process these and save the spectra in binary files which then could be read for further analysis by other software packages already existing in IDL and software which had to be developed.

4.2 Optical Data and Software

For the ASK data a software package developed by the University of Southampton and Alfvén Laboratory exists. This software package contains simple viewing scripts up to specialized routines. The software package is written in IDL and some of the scripts were modified to analyze this data set.

In the following also figures showing the intensity of the three imagers are used. These figures have been produced with an existing script integrating the intensity over the radar field of view, i.e., a circle of 1° . The intensities are then shown in line plots with the intensity vs. time.

4.3 Overview of Data

In Figure 4.1 an overview of the radar data is shown where the lower panel is the returned power and the upper panel the electron density. In the bottom of this Figure colored inlays are shown which show heater on times, red corresponds to O-mode heating and blue to X-mode heating. In the beginning of the experiment (16:40 - 17:40) the heater was operated in a continuous mode i.e. the heater was on during the 2 min cycle time. At 17:40 the operating mode was changed from continuous to 2 min cycles of 10 Hz modulated (on - off) heating of the ionosphere.

As stated above the experiment site is located close to the statistical auroral oval. On the day of the experiment the ionospheric conditions are disturbed and during the experiment auroral arcs passed the ionosphere above the experiment site. Especially during 18:10 and 18:30 strong activity can be seen in the radar data, see Figure 4.1. Later on the activity is getting weaker and the ionosphere more stable. In the end of the data set a sporadic E-layer crosses the radar beam (19:54 - 19:58). Besides this also a change in the background ionosphere goes on. From the beginning of the experiment until about

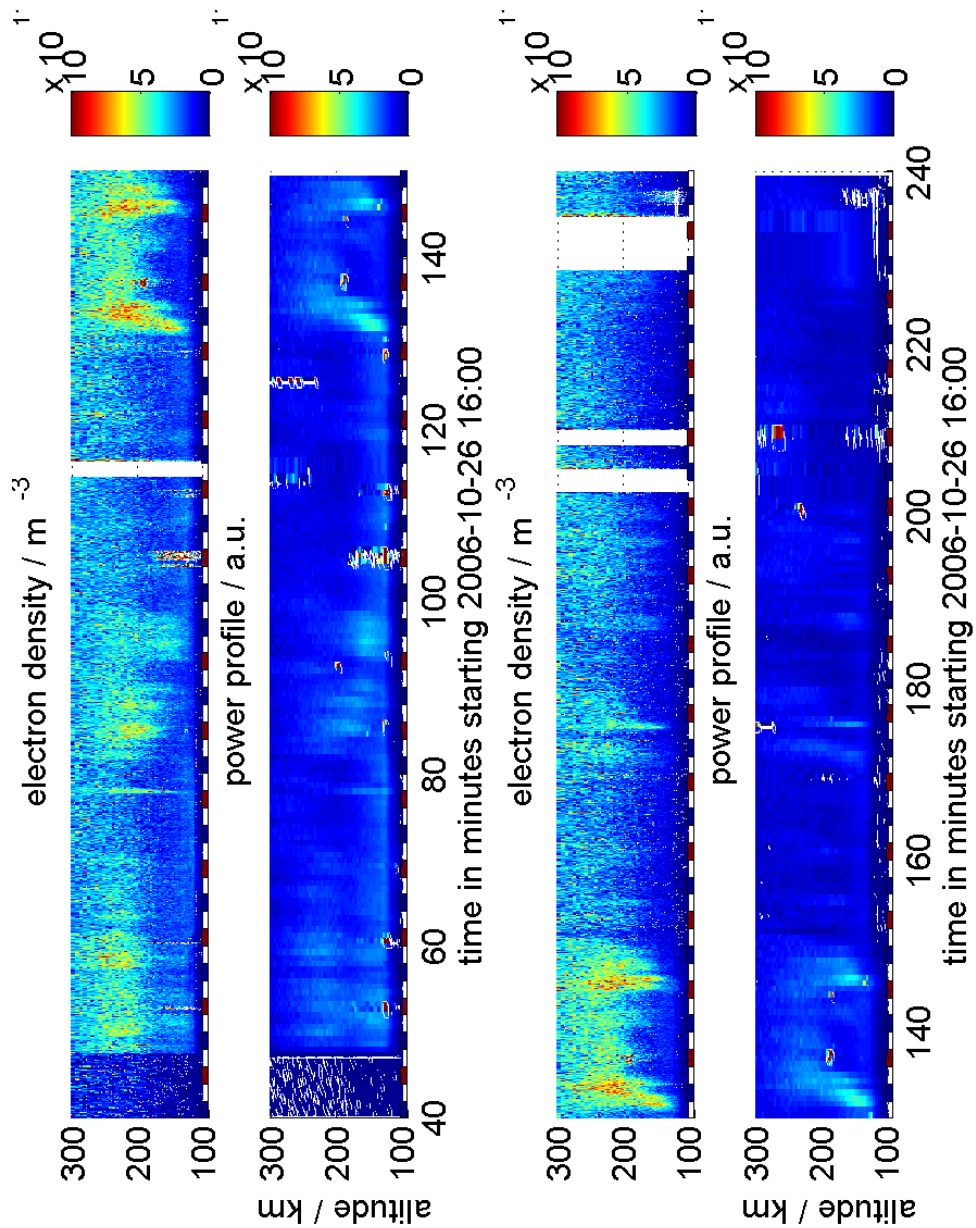


Figure 4.1: Overview plot of the radar data showing power profiles in the bottom panel and electron density in the upper panel. The colored bars indicate heater on where red corresponds to O-mode heating and blue to X-mode heating.

17:30 the ionosphere contains a E-layer which peak density decreases during this time and disappears completely later on due to sunset at 16:41(at sea level)[TimeandDateAS, 2010].

In some of the heating cycles a rise in the electron heating is observed. This phenomenon is well understood and has been of scientific interest many years. A general review of the interaction experiments of powerful HF-waves with ionospheric plasma is given by Leyser and Wong [2009].

For this thesis I will concentrate on heating cycles with enhanced response from narrow altitude layers seen in the radar, e.g., during the heating cycle 17:44-17:46. Below a list of such enhanced responses is given to get an overview of available data and ionospheric and auroral conditions. Some of the details given below are not obvious or can not be seen in the overview Figure and more analysis was done for this descriptive overview. However it is not possible to show all Figures here. Also the spectral characteristics are not shown for all events. Nevertheless a brief description of the ion line spectra will be given. For making the description easier the spectra are described either as three ion lines (TIL) where the three lines represent the two ion lines and a central line or as not resolved (NR). The name “not resolved” might not be the correct interpretation of the spectra but is however useful. An example for TIL and NR is shown in Figure 4.2. As stated before, no plasma line data have been recorded.

The description of auroral activities seen with the ASK instrument is valid for all three cameras unless stated explicitly.

In the listing of enhanced responses below only heating cycles with O-mode heating are mentioned, this is because only for O-mode waves the swelling of the heater wave (see section 3.2 in chapter 3) occurs. The swelling increases the electric field strength of the heater wave close to the reflection altitude and therefore exceeds the threshold for instabilities more easily. Those O-mode heating cycles with no enhancements are listed to give a better overview of physical conditions.

Heating in 2 min cycles and mode inversion every 4 min.

- O1 16:52-16:54

Radar: During the first seconds of heating a plasma instability is triggered close to the critical density for the heating wave and is seen as enhanced power in the power profile. The density in the E-layer decreases and the heater wave propagates higher up and / or is absorbed. Approximately 30 s later at 16:52:29 the density in the E-layer gets close to critical again and once more plasma instabilities are triggered, the IL spectrum is of the TIL type. Some seconds later the altitude of insta-

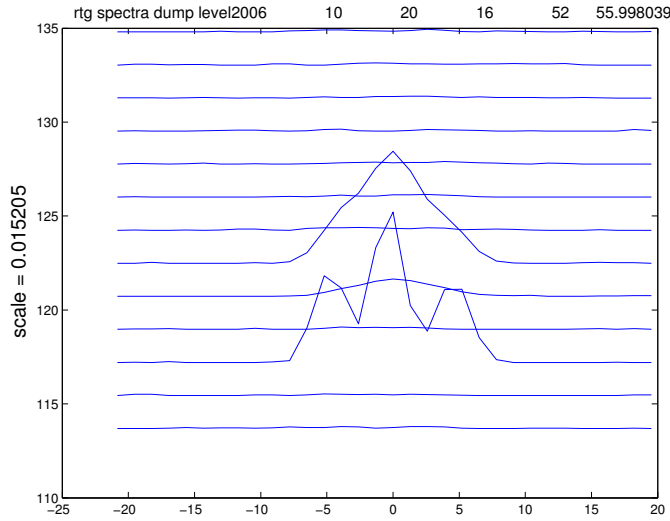


Figure 4.2: Computed ion line spectra of the two typical spectra. On the abscissa the frequency is plotted and on the ordinate the strength for different altitude bins is shown i.e. each line corresponds to one altitude given by the ordinate. The spectra for each altitude bin are normalized to the same value. In the upper layer with enhancement a typical NR spectra is seen with a strong central ($\omega = 0$) feature and small not resolved shoulders. The lower layer at about 118 km altitude shows a TIL spectra. Clearly three spectral lines are resolved with a central line and two lines at about ± 5 kHz corresponding to the UIL and the DIL.

bility decreases slowly and a second layer of enhanced returned power is seen about 5 km above with NR spectral characteristics. After some seconds of coexistence the lower turbulent layer disappears and some seconds later also the upper layer vanishes. Despite density being close to critical or even overdense no further turbulence is observed. Below the E-region peak as seen in Figure 5.1(a) an increase in electron temperature is observed during the heating cycle.

The two distinct layers of turbulence are discussed in more detail in the section 5.1.

Optics: About five minutes before the heating cycle (17:45-17:49) fast changing aurora is seen with the ASK instrument. The aurora also shows small structures with scale sizes of the radar beam width. During the heating cycle the aurora is diffuse and except for a less intense bar passing 18 s after heater turn on no structures are observed. Irregularities

and structures are passing from north-east to south-west. A plot of the auroral intensity across the radar beam is given in section 5.1 for all three imagers.

- O2 17:00-17:02

This heating cycle begins with plasma instability at about 120 km which also corresponds to an altitude with electron density close to critical. At this altitude the instability is seen over about 20 s and 10 s after heating begin even a second layer of turbulence is seen at about 6 km below the first turbulent layer. Again the upper layer is characterized by the NR spectra and the lower layer of turbulence by TIL. First the upper layer disappears about 20 s and the lower layer at 25 s after heater on. Later on short enhancements in returned power are seen at the altitudes of the two layers before. Compared to cycle O1 the electron temperature below 120 km increases even more during this cycle.

This heating cycle will be analyzed in more detail in section 5.2.

Optics: During this heating cycle a diffuse arc is passing the radar beam between 17:00:38 and 17:00:42 in the north-east to south-west direction as seen with all three imagers. The data also reveal weak an arc passing at 17:01:01 more clear to see in ASK2 and ASK3. Later on at 17:01:17 a diffuse boarder crosses - in the same direction - with stronger aurora afterwards. A plot of the auroral intensity across the radar beam is given in section 5.1.

- O3 17:08-17:10

Only a short enhancement of returned radar power is observed 80 s after heater on afterwards the E-layer electron density is just below critical. The electron density is slightly above 10^{11} m^{-3} between altitudes from 110 to 250 km increasing slowly. Therefore the heater beam might be bent slowly, reflected and absorbed.

Optics: In the ASK image data no structures or enhancements are seen in area of the radar beam. From 17:09:50 on a very weak arc is close to the southern boarder of the radar beam till the end of the heating cycle.

- O4 17:16-17:18

The electron density in the E-region is below critical and no enhancements are observed. At the end of the heating cycle at about 17:17:30 an auroral arc enters the radar beam until about 17:18:30 which is seen in the radar data (Fig. 4.1) and in ASK optical data (not shown here).

Optics: A very intense auroral arc is crossing the field of view of the ASK instrument during this heating cycle. The intense center of the

arc is crossing the radar beam between 17:17:45 and 17:17:55 and has width of about $1.5 \times$ beamwidth. This arc corresponds to the increase in electron density as seen in the radar.

- O5 17:24-17:26

Before this heating cycle at about 17:22 weak electron precipitation above 160 km starts with changing intensity and altitude. During heating the altitude in the E-region with electron densities close to critical is at 150 km. In the power spectra it can be seen that two different altitude regimes exist where enhanced power is observed. The time development of these two layers are kind of alternating due to close to critical electron density in the lower E-region. The first enhancements which are strong enough for good spectral data analysis are 15 s and 30 s after heater turn on for E-region and F-region. Both of these events are more of the NR type with strong central features. The other events at 50 s and 90 s are of the TIL type with three distinct spectral lines.

Optics: Prior to the heating cycle starting at about 17:23:55 auroral activity is seen in the northern edge of the ASK field of view. In the beginning a precursor reaches the radar beam the main part of the active region at 17:24:15. At 17:24:40 a less intense area is crossing the radar beam followed by aurora with water wavelike structures till the end of the heating cycle. The direction of the structures passing is from east to west.

- O6 17:32-17:34

The auroral event from the above heating cycle is still going on. In the first half of the heating cycle electron precipitation is rather weak and the E-region electron density is well below critical. At heater turn on a very short event (≤ 1 s) is observed in the F-region at 190 km. The enhancement is spread over approximately 5 km in altitude and the lower part is of TIL type where as the upper part is of the NR type. After about 1 min at 17:33 electron precipitation increases again leading to a overdense E-region and in consequence 10 s of intense turbulence are observed with enhancements in returned power just above noise the following 20 s. Spectra are of the NR type.

Optics: Prior to the heating cycle measured auroral activities are rather low with an increase at 17:32:48 where an active region is fading into the beam. Around 17:33:45 north and partially in the radar beam structures move westward and at the southern border of the beam structures move eastward with low intensities inbetween.

Change in heating mode from 2 min cycles to 2 min 10 Hz modulated cycles

- O7 17:44-17:46 As stated above during the following heating cycles the heater is operated in a 10 Hz modulated mode.

This cycle is characterized by a layer of enhanced returned power during almost the whole 2 min of heating. The electron density in the E-region is above or close to critical leading to heater induced instability at ~ 120 km. Because of high backscatter power and the use of a phase coded radar program no further analysis of the radar data can be done during times with turbulence i.e. electron density and temperature are only available before, after and for a few seconds of this heating cycle. In the available electron temperature data no electron heating below reflection is seen. The spectral characteristic is changing and in the first part until the short interruption at about 25 sec is more of the NR type and afterwards of the TIL type. At times when the layer lies within two altitude bins the lower part has a less intense central line compared to the upper part of the layer. Further analysis of this cycle is given in section 5.3.

Optics: Irregularities in intensity are seen previous to the heating cycle and in the first 5 s. The rest of the cycle is characterized by wavy structures passing from east to west. In section 5 Figure 5.11(b) shows the observed intensities. The enhancements in auroral emissions in this Figure correspond to structures in the active region passing the radar beam.

- O8 17:52-17:54

As well as during heating cycle O7 the induced turbulence is rather constant during this cycle. Starting with the onset of the heater at about 120 km altitude with slight altitude variations and close to the critical density. In the second half of the cycle the E-region density decreases with consecutive vanishing turbulence. During the first 40 s spectra show a very strong central feature whereas the spectra later on also show resolved ion line peaks. At the end of the cycle single events of enhanced power are recorded at the same altitude.

Optical data reveals rather constant auroral conditions with slightly decreasing intensity and small structures. This cycle will be represented with more details in section 5.4.

Optics: ASK image data show low intensities with less intense bars in east-west direction passing the field of view in north-south direction. In section 5 Figure 5.16(b) shows the intensities observed with the three cameras across the radar beam.

- O9 18:00-18:02
 During this cycle electron density is almost monotone increasing to altitudes of 250 km and higher and no clear over critical E-region peak seen. Also auroral conditions are quiet. No enhancements are observed.
Optics: No activity.
- O10 18:08-18:10
 Compared to the O-mode heating cycle described above the electron density in the E-region increased again leading to heater induced turbulence in the E-region. While in the above listed heating cycles the returned power of the turbulent layers is above noise and clearly to see in the power spectra the returned power during this cycle is sometimes close to noise level and only seen with time integration.
Optics: After very low intensities in the beginning at 18:09:10 strong activity - specially seen with ASK1 - is seen at the northern edge of the image data. The activity increases and fades into the center of the ASK field of view and the radar beam. The strongest activity is reached at about 18:11 with the end of the event around 18:14. Structures during this event move from west to east.
- O11 18:16-18:18
 This heating cycle differs from the heating cycles before because it's the only cycle with rather continuous turbulence in the F-region. The ionosphere is characterized by very low electron density in the E-region - below $10^{11} 1/m^3$ - and auroral electron population in the region above 160 km. Enhancements in the backscattered power are measured for more than 1 min with more spreading in altitude than for the events listed above and again rather weak enhancements. Due to the fact that the electron temperature in the F-region is typically higher than in the E-region the ion line frequencies are also higher - see equation (3.29). In our case the ion line frequency for this altitude is about 10 kHz leading to well resolved spectra with ion lines and a central line.
Optics: Low activity during this heating cycle.
- O12 - 23
 From 18:30 to the end of the experiment at 20:00 the ionosphere got more quiet with weak and less intense electron precipitation. Consecutive the ionospheric electron density profile is more smooth and flat without high gradients. During this time only a few and very short events of turbulence (~ 1 s) are observed in the F-region.

- 19:54 - 19:58 In the end of the heating experiment a sporadic E-layer passed the region above the Experiment leading to enhanced radar echoes during this time. Also the heater was operated from 19:56 till 19:58 in X-mode.

Chapter 5

Parametric Decay Instability in the auroral E-region

As described in the previous section during the heating experiment plasma instabilities were triggered in the E-region as well as in the F-region. In this section we will take a closer look on some of the events with enhanced returned radar power from the E-region.

5.1 Heating cycle O1

This is the first O-mode heating cycle starting at 16:52 and ending at 16:54 after 2 min of continuous heating. Radar data of this heating cycle are shown in Figure 5.1(a). Due to the use of a phase coded radar program the data set during strong enhancements is not useful for further analysis e.g. electron density. This can be seen in the power profile as noisy data at altitudes above and below enhancements. Panels in Figure 5.1(a) with physical properties are therefore without data during such times.

After ~ 1 s till ~ 6 s instability is triggered at 122 km with three orders of magnitude higher power in the returned radar signal at the beginning of the instability. The signal then decreases to the end of the event and returns to normal power, see the top row of plots in Figure 5.2. The spectra of this short event are of the NR type as described in section 5 and illustrated by Figure 4.2.

From 16:52:29 on at the same altitude as before (122 km) a second enhancement is observed until 16:52:54. The altitude of the layer is decreasing during the first 10 s to an altitude of 118 km. Integrating the power of the enhanced layer over altitude reveals again a quick rise (~ 1 s) of returned power by three order of magnitudes and then decaying to the end. Unlike during the

first enhancement the IL spectra show three distinct lines.

At 16:52:45 a third enhancement about 5 km above the previous enhancement appears lasting till 16:53:07. Hence two layers of enhancement exist for 10 s and will be referred to as upper and lower layer. Contrary to the lower layer the upper layer spectra are of the NR type, see Figure 5.3.

The spectra discussed here were obtained using the `rtg` program to calculate and save in binary files. In order to summarize the spectral details in a more illustrative way the spectra of altitudes with enhancement were fitted with three gaussian curves. Where the three parameters shown in Figure 5.2 are determined by:

$$G(\omega) = \frac{A}{\sqrt{2\pi}\sigma} \exp[-(\omega - \omega_0)^2/(2\sigma^2)]. \quad (5.1)$$

Plotted are the amplitude A , the center frequency ω_0 and $\sqrt{2\pi}\sigma$ which is proportional to the width. Blue indicates the lower layer, red was chosen for the upper layer and for the event at the beginning of the heating cycle due to the similarities in the IL spectra.

The amplitude of the lines compared to the center frequency gives the impression that these two parameters are coupled to each other. Also the width of the spectral lines is decreasing with decreasing amplitude which is clearly seen for the lower (blue) layer. However the upper layer with in general smaller amplitude reveals higher widths. Interesting to state is also that the center frequency of the central ion line (CIL) which is usually at $\omega = 0$ drifts to negative values (-0.5 kHz) at the end of the event. This could be due to a movement of cavitations, however the spectral resolution is only about 1.3 kHz and the data set should not be over interpreted.

Out of Figure 5.2 it might be difficult to distinguish between the two different layers but Figure 4.2 clearly shows the difference of the upper and lower layer.

Power profile: Because of no useful electron density data could be computed while ongoing turbulence using standard programs such as `guisdap` a different procedure was used. The power profiles were modified so that they represent the electron density as best as possible. Therefore the averaged power profiles were compared to averaged electron density data computed with `guisdap` before and after the event of interest:

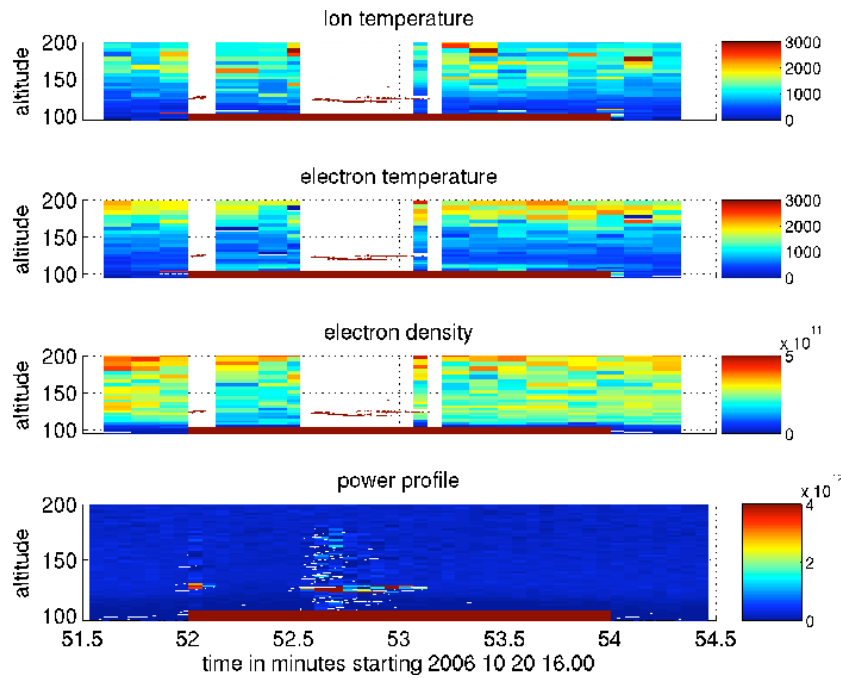
$$\text{electrondensity} = \text{powerprofile} \cdot g(h), \quad (5.2)$$

where $g(h)$ is a weighting factor. In Figure 5.5 such modified power profiles are shown where the blue solid line corresponds to the modified power profile

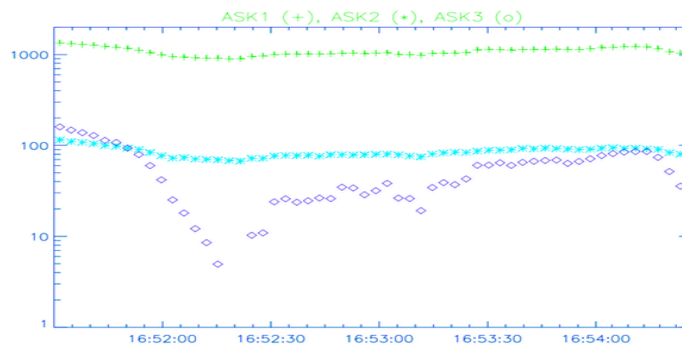
and the blue dashed line to a polynomial fit of 5th order. Furthermore each Figure shows a blue and red asterisk. The red asterisk corresponds to the critical density and altitude according to the fitted curve whereas the blue asterisk is placed at the altitude of the matching height, see section 3.4.

The plots shown in Figure 5.5 were chosen to represent the ability of the procedure described above. It shows two plots at the bottom where the critical density is close to or at the same altitude of one of the turbulent layers and the matching height lies at the altitude of the lower turbulent layer which occurred in many cases. However the two plots at the top show that this process was not easy and that the layers not always coincided with the calculated altitudes. The main problem is the same as for standard software to fail the use of a coded radar program.

Electron density profile: In order to get a satisfactory density profile time or altitude averaging has to be done. Since auroral processes were going on during the experiment changing the density this averaging has to be done with care. For this heating cycle the time of integration has been chosen to start during the heating cycle right after the events of turbulence at 16:54:30. The result is shown in Figure 5.4 and it shows two local peaks in the E-region at 115 km and 132 km altitude. As seen at higher altitudes these peaks might not be the result of the electron profile but could be noise as seen also higher up. However as mentioned earlier in section 4 data from low altitudes usually have a better SNR since less reflected power is received from higher altitudes with the radar.



(a)



(b)

Figure 5.1: a) Radar data during heating cycle O1. The panels show Ion temperature, electron temperature, electron density and the power profile. On the bottom of each panel a red bar indicates heater on. In the upper three panels red polygons represent altitudes of enhanced backscattered power. b) Observed intensities with the three ASK imagers integrated over the width of the radar beam.

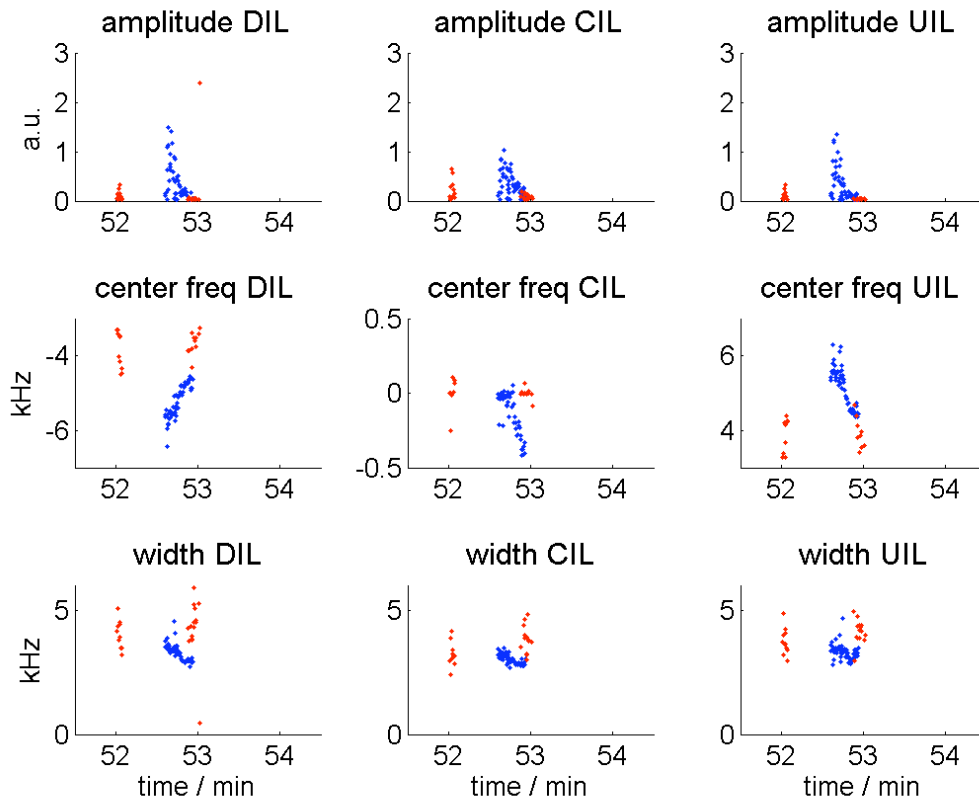


Figure 5.2: Spectral characteristics of enhancements during heating cycle O1. Plotted are the parameters of three fitted gaussian curves to the IL spectra. The columns show the downshifted ion line (DIL), the central line (CIL) and the upshifted ion line (UIL). Rows are amplitude (a.u.), center frequency in kHz and width in kHz of the fitted gaussian curves. Blue data points refer to the lower layer, red to the upper layer and the event in the beginning of the heating cycle.

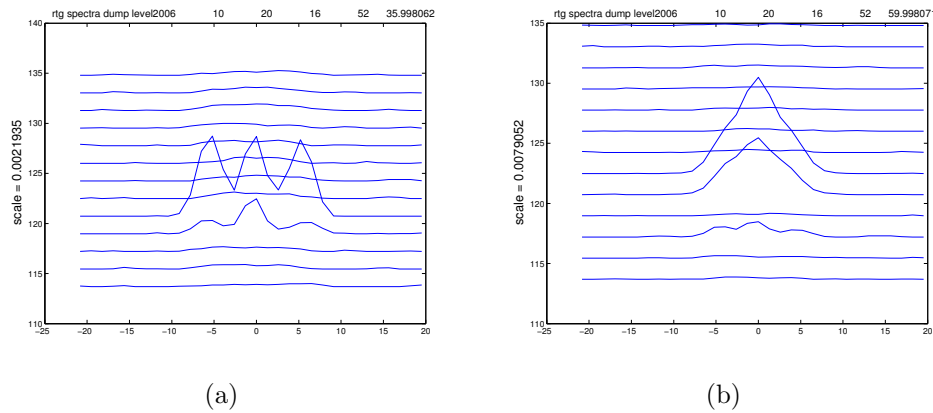


Figure 5.3: Computed ion line spectra for heating cycle O1. The line plots show amplitude vs. frequency (abszissa) at there corresponding altitude (ordinata). The amplitude is normalized to the highest value occurring in one plot and the scale is noted at the ordinata. a) for the dump ending 16:62:36 and b) for the dump ending 16:53:00

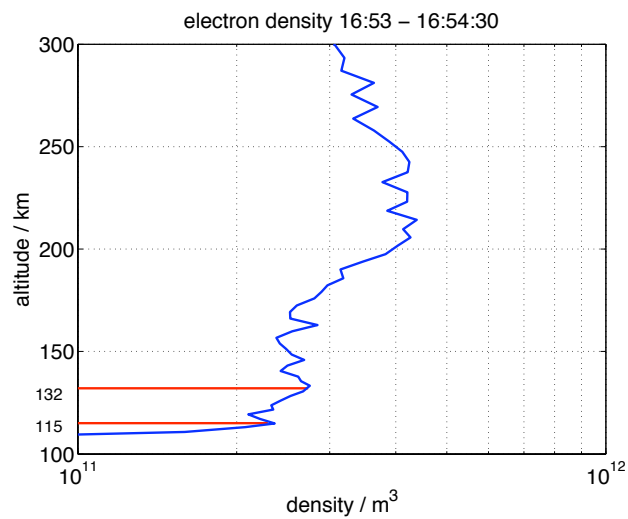


Figure 5.4: Average of electron density data (blue line) close to heating cycle O1. Electron density data has been averaged between 16:53:00 and 16:54:30. The two horizontal red lines indicate local peaks in the density profile at 115 km and 132 km altitude.

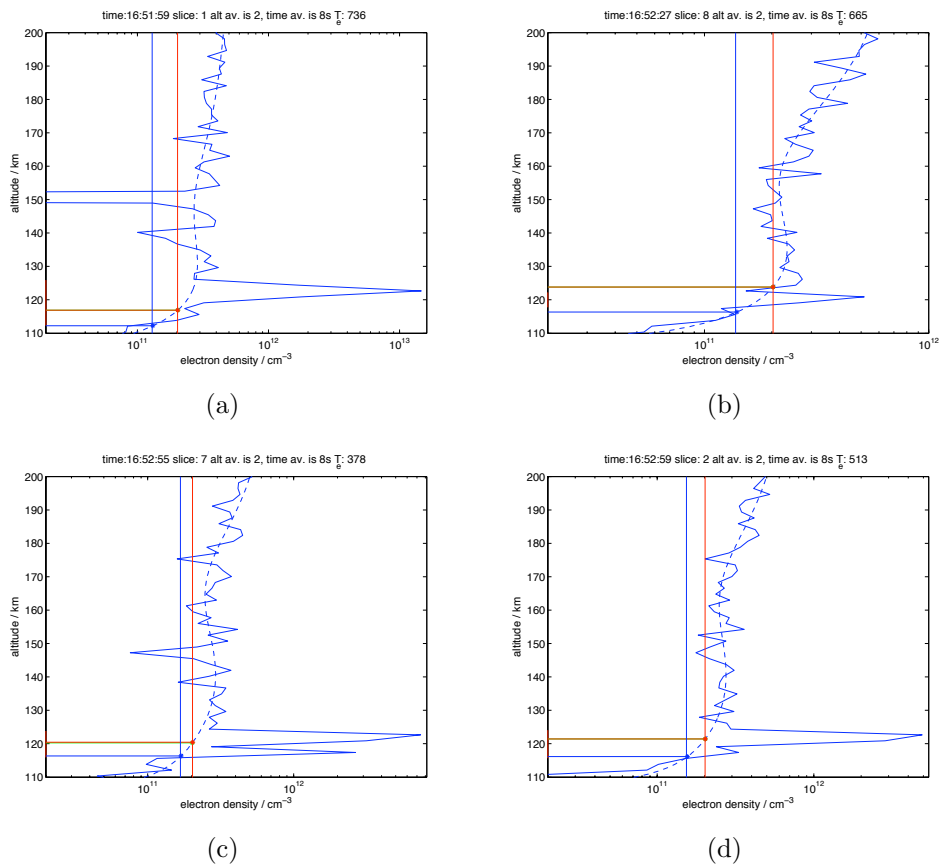


Figure 5.5: Modified slice power profiles (see eqn. 5.2) during heating cycle O1 showing enhancements of up to two orders of magnitude in the returned power. The blue solid line corresponds to the modified power profile and the dashed blue line to a 5th order polynomial fit. Figure 5.5(c) shows the appearance of two layers of enhancements at the same time.

5.2 Heating cycle O2

During heating cycle O2 continuous O-mode heating was done for 2 min as before during heating cycle O1.

Approximately 5 s after heater on enhancement at 125 km altitude is observed and lasts till 17:00:27. Just 3 s after the first layer appears a second layer of enhancement ~ 5 km below and is detected till 17:00:31. Again the upper layer of enhancement is characterized by spectra with a strong central line and non-resolved ILs. The lower layer is characterized by spectra with two well resolved ILs and a central line. During this time of enhancements and also later on for a couple of seconds the decoded data is disturbed and no useful data analysis could be done.

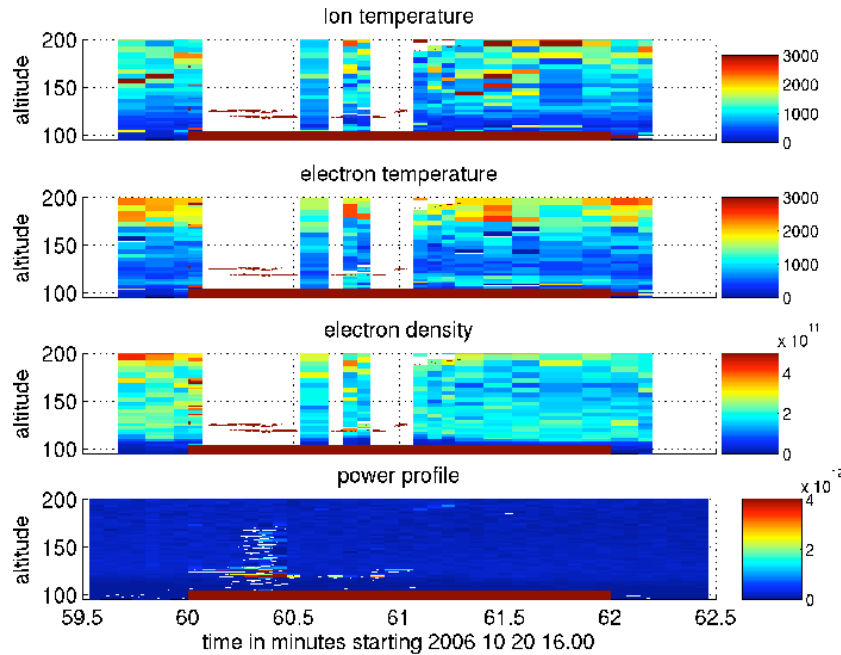
At the altitude of the lower layer enhancements continue till 17:00:52 with interruptions in between. Also at the altitude of the upper layer enhancement is seen from 17:00:57 till 17:01:03.

In the analyzed data it can be seen that the electron temperature rises after about 17:00:40 below the E-region which can be interpreted as higher absorption in this region.

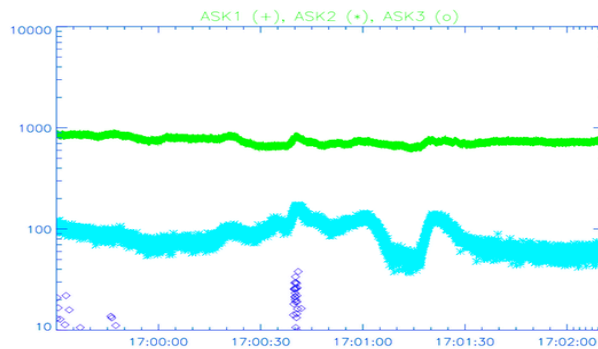
Not shown in Figure 5.6(a) is the altitude above 150 km where between 17:01:04 and 17:01:19 enhancement of the returned power is seen at approximately 190 km as described in section 5.

This heating cycle has more data points with both layers at the same time due to longer time of coexistence and more data points within the predefined maximum fitting error. The decay of the lines taken into account for the fits is not as strong as in the case for heating cycle O1. Also a change of the parameters for the width and the center frequency with time is not noticeable for this heating cycle. However in the plot for the center frequencies the upper and lower layer are still to distinguish with an average center frequency of about 4 kHz for the upper (red) and 5 kHz for the lower (blue) layer. The parameter for the width of the lines is also different for the two layers. Still it has to be taken into account that the amplitude for the lines of the two layers is not the same. Two spectra of this heating cycle showing the upper and the lower layer are shown in Figure 5.8.

Power profile: As described previously to overcome the problem of non-available data for physical properties during strong enhancements the power profile was modified to represent electron density. The result for this heating cycle is shown in Figure 5.10. The first plot shows the first layer above 120 km continued by the second layer below 120 km. And in the last plot just the lower layer remains. During this heating cycle the approximated critical density coincides well with the top layer. Also the lower layer with the matching



(a)



(b)

Figure 5.6: same as Figure 5.1 for heating cycle O2.

height which will be discussed in section 6.

Electron density profile: Compared to the electron density profile shown for heating cycle O1 (Fig. 5.4) a longer integration period could be used for this profile leading to a better SNR. Electron density data between 17:02 and 17:08 has been averaged to obtain the profile shown in Figure 5.9. This was possible due to a rather stable density distribution in the E-region, also seen in Figure 4.1. Again the profile has two peaks in the E-region this time at

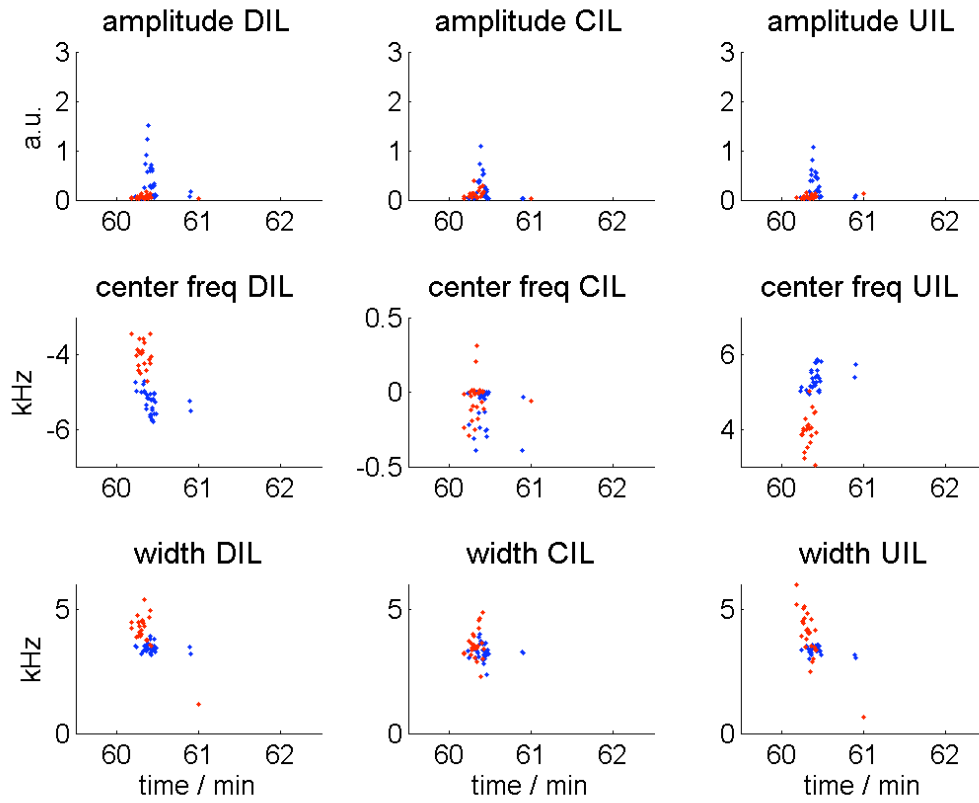


Figure 5.7: Same as Figure 5.2 for the second O-mode heating cycle.

115 km and 127 km altitude.

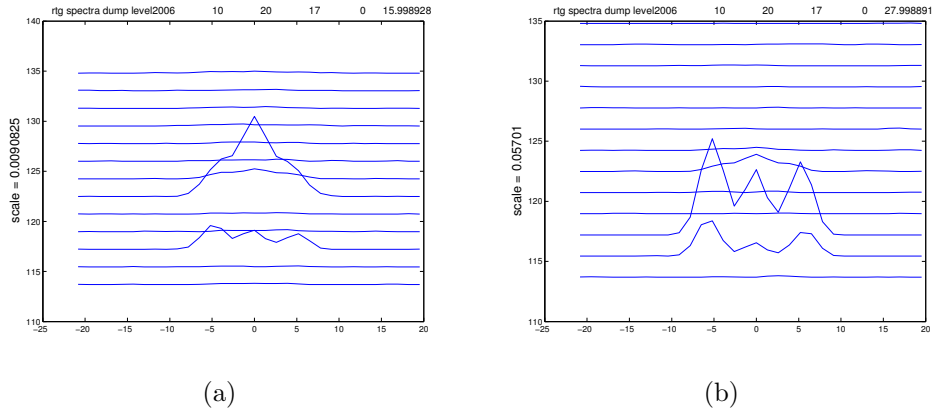


Figure 5.8: Plots showing spectra for heating cycle O2 the same way as Fig. 5.3. a) for the dump ending 17:0:16 and b) for the dump ending 17:0:30.

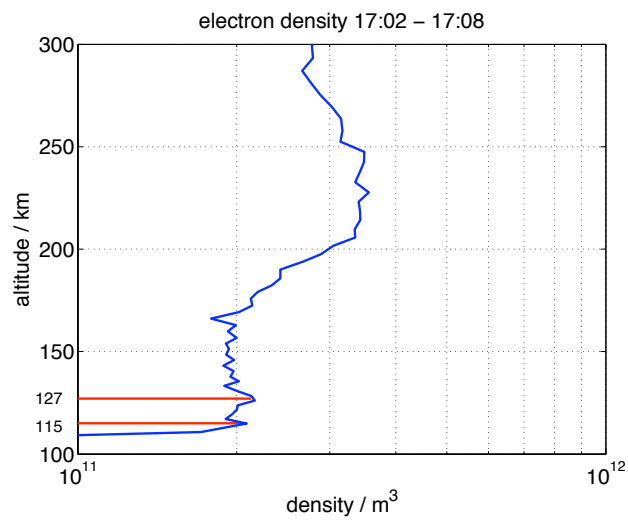


Figure 5.9: Same as Figure 5.4 for the time after heating cycle O2 showing the electron density profile averaged between 17:02 until 17:08. The two horizontal red lines indicate local peaks in the density profile at 115 km and 132 km altitude.

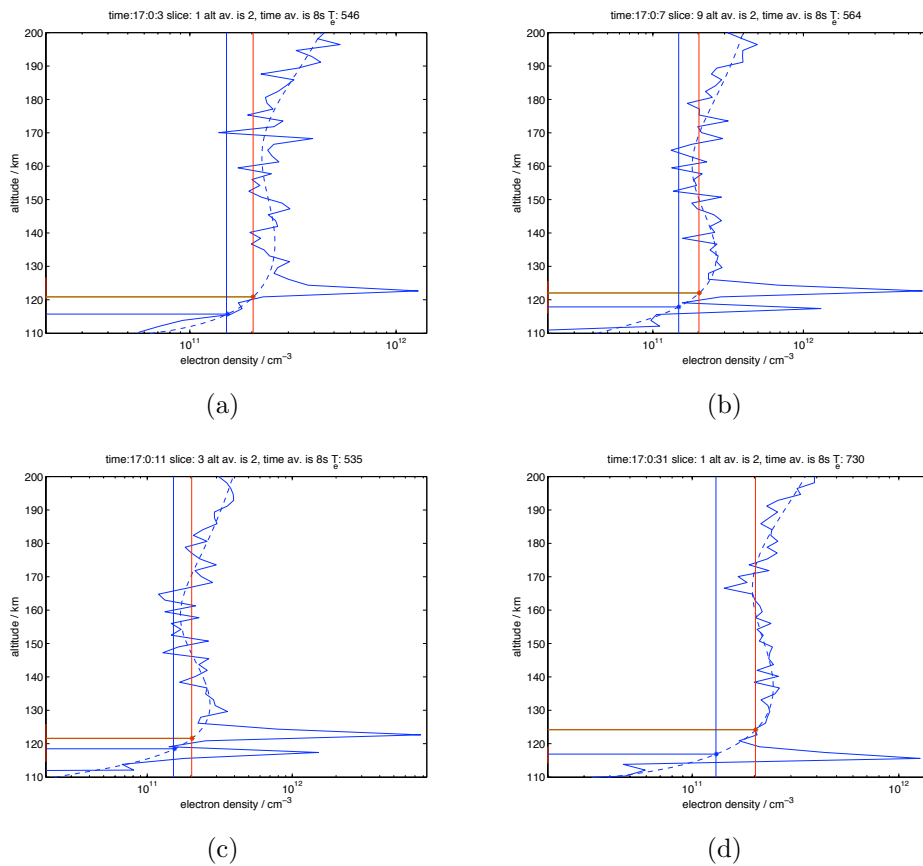


Figure 5.10: Same as Figure 5.5 for heating cycle O2. Figures 5.10(a) to 5.10(d) are placed in chronological order. In Figure 5.10(c) the upper layer of enhancement appears. Later on (Fig. 5.10(b) and 5.10(c)) two layers with enhancement are observed simultaneously. In the end of the event only the lower layer is seen in the power profile.

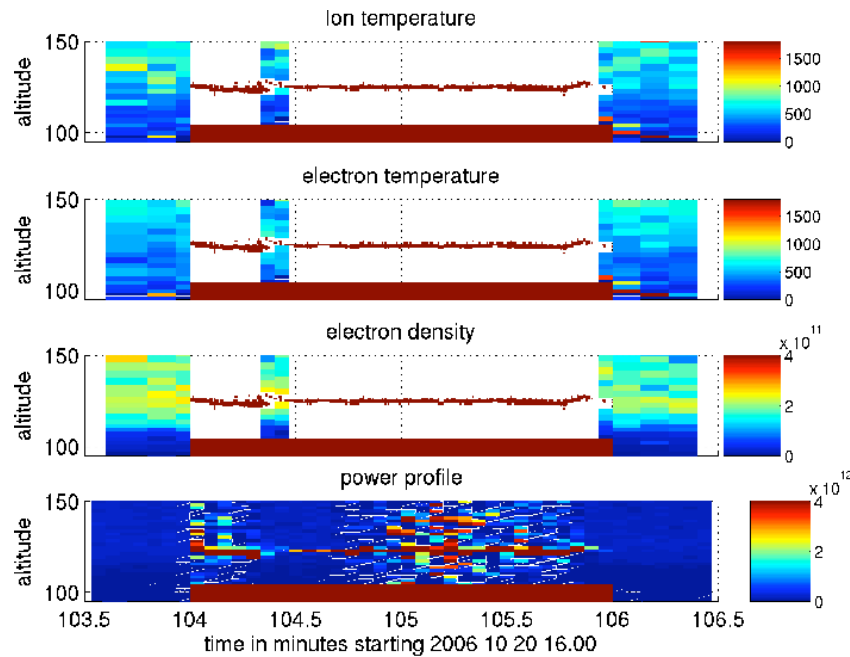
5.3 Heating cycle O7

As seen in Figure 5.16 this heating cycle is characterized by strong enhancements in the returned power during almost the whole 2 min of heating. Therefore no useful analysis leading to electron density and temperature is possible. Compared to the heating cycles discussed above the heater was not operated in a continuous mode. Instead the heater was operated with 10 Hz on-off modulation. The resulting period of modulation is 0.1 Hz which is considerably less than the time resolution of the decoded radar data. Hence no comments regarding the characteristic of triggered instabilities on time scales of the modulation can be done.

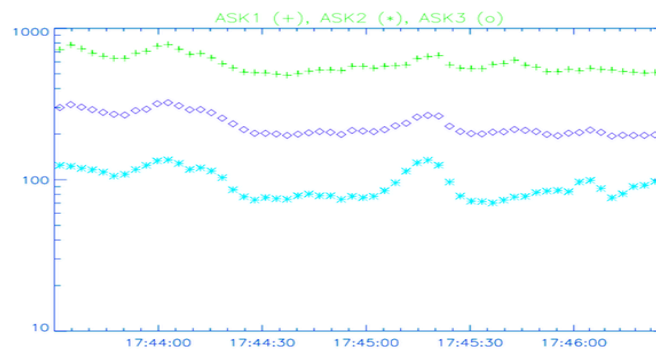
The enhancement of the returned radar power is detected from the first dump until approximately 17:45:55. At 17:44:20 the enhancement has a dip and gets weaker for about 5 s. Compared to the other discussed events of enhancement this one is very steady also in terms of altitude variation. The enhancement starts at 125 km and stays at this altitude with small variations as seen in Figure 5.11(a). As stated above this event is characterized by strong enhancement in the returned power making it impossible to get useful data for the plasma properties. However in the analyzed data previous, afterwards and during the dip in returned power at 17:44:20 no rise of the electron temperature below reflection is observed. Also the electron temperature in the E-region (≈ 500 K) is below observed values therein during the heating cycles discussed above (≈ 900 K).

In Figure 5.11(b) - showing the observed auroral emissions - it is seen that the three lines show similar behavior during this heating cycle. During the beginning of O7 and at 17:45:25 the auroral activity across the radar beam is rising for several seconds. A closer look at the image data which is not shown here reveals that the aurora is wavy and soft but with structures. The movement of irregularities and structures is from east to west.

Characteristics of the ion line spectra as shown in Figure 5.13 are summarized in a separate Figure (Fig. 5.12) as before. Generally spoken the spectra shape of the turbulent regions is of the TIL type showing two ILs and a central line well resolved. The center frequency of the ILs are at around ± 4 kHz for the first 30 s. Afterwards the center frequency rises to values above 4 kHz getting lower again in the very end. The width of the three spectral lines during the whole 2 minutes is just below 4 kHz. Comparing the amplitudes of the lines shown in Figure 5.12 with the auroral intensities shown in Figure 5.11(b) shows a correlation of these properties. This correlation is also valid for the shape of the spectra in that case that the central line is more dominant during times with higher optical intensities. However this is the only heating cycle where a correlation has been found.



(a)



(b)

Figure 5.11: Same as Figure 5.1 for heating cycle O7.

Power profile: Shown in Figure 5.15 are power profiles during times of rather low enhancement for this heating cycle. Compared to previously shown power profiles the peaks of enhancement are rather wide showing even a small dip in some of them as seen in Figure 5.15(b).

Electron density profile: To obtain the density profile it was chosen to average electron density data between 17:47 and 17:49. The profile shown in Figure 5.14 has only one clear peak in the E-region where the turbulent

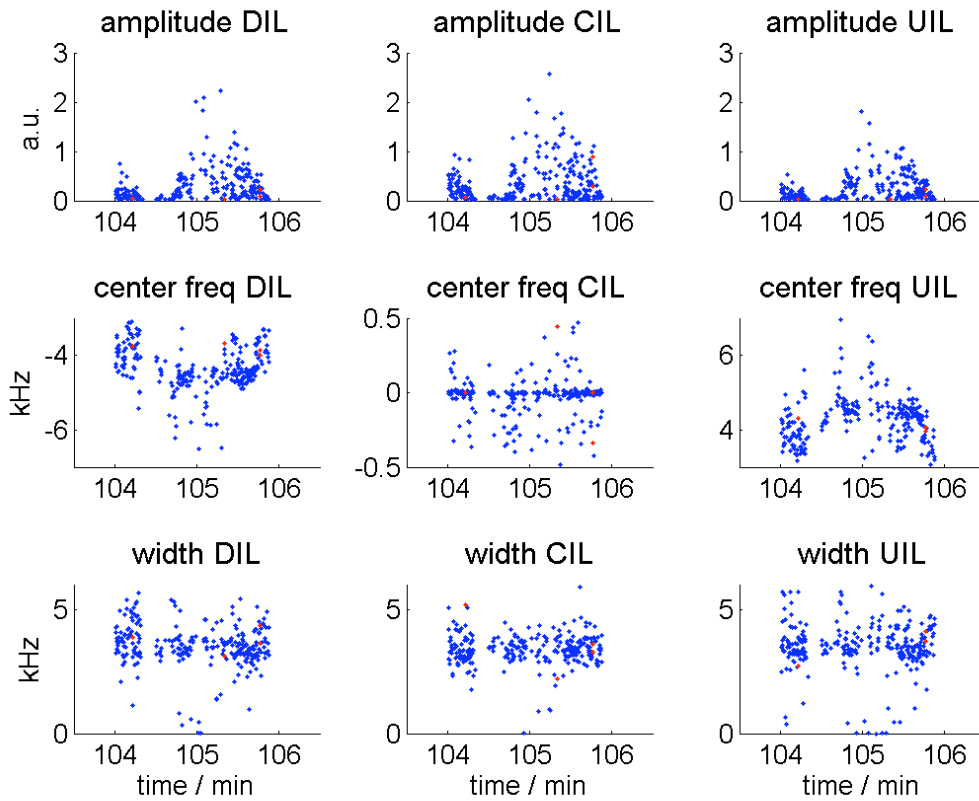


Figure 5.12: Spectral characteristics of enhancements during heating cycle O7, same as Figure 5.2. Although two separated layers are not observed the automated analysis program categorized some of the data points as a separated layer marked red.

events had been observed. The peak is again indicated by a red line at 125 km altitude.

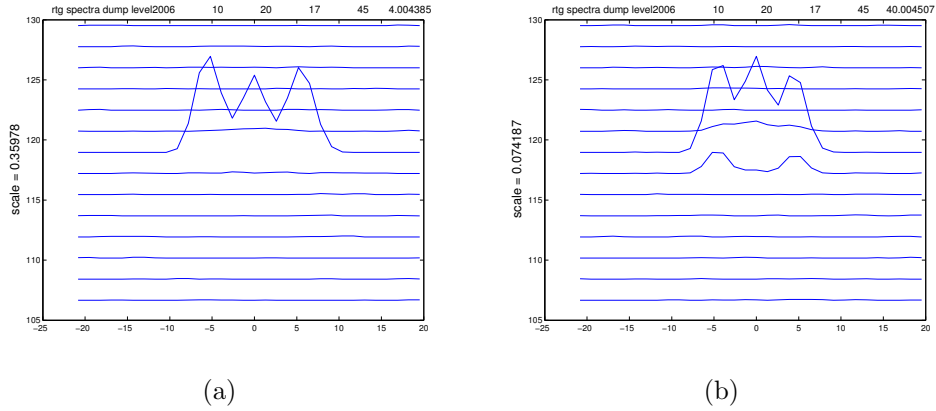


Figure 5.13: Same as Fig. 5.3 for heating cycle O7. a) for the dump ending 17:45:4 and b) for 17:45:40.

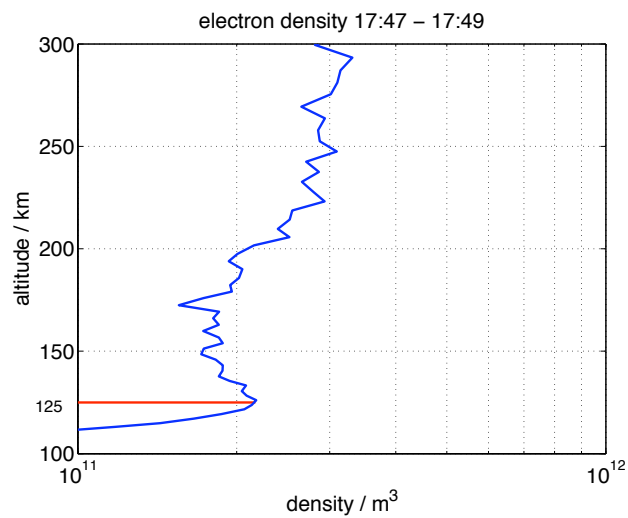


Figure 5.14: Same as Figure 5.4 for the time after heating cycle O7 showing the electron density profile averaged between 17:47 until 17:49. The horizontal red line indicates the local peak in the density profile at 125 km altitude.

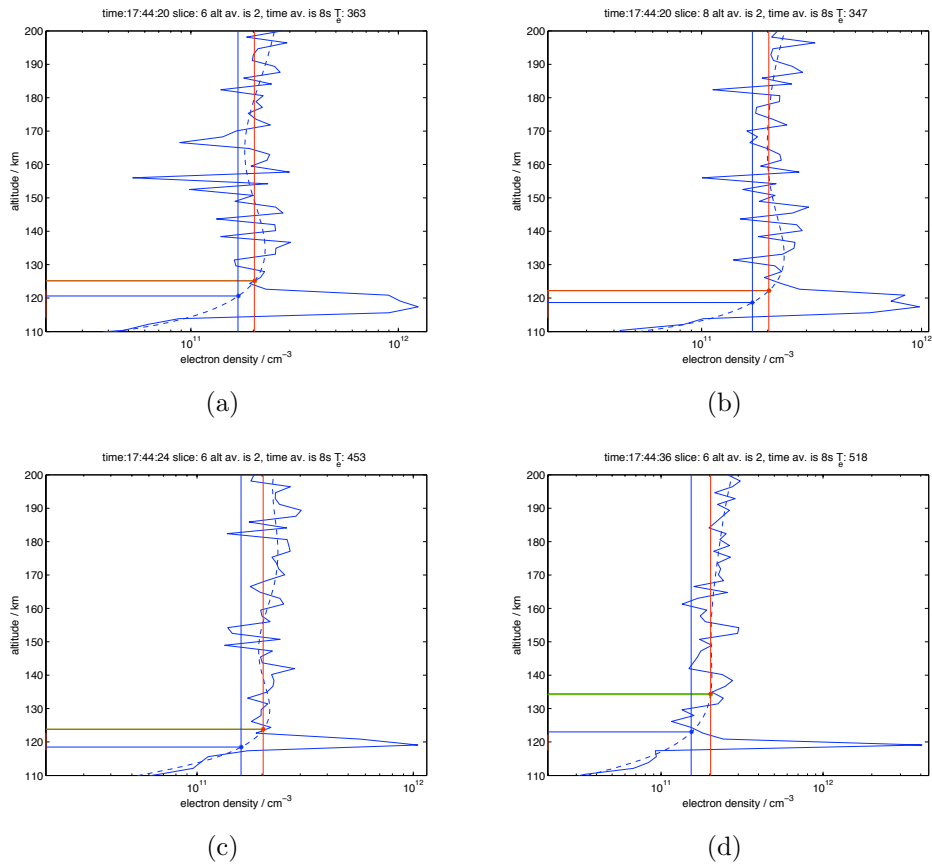


Figure 5.15: Same as Figure 5.5 for heating cycle O7. Because of the strong enhancement during most times of the event the power profiles shown here has been chosen to show times of enhancement with rather low "decoding noise".

5.4 Heating cycle O8

For this heating cycle the same 10 Hz modulation as for heating cycle O7 was used.

This heating cycle gives a more stable enhancement than O1 and O2. However compared to the previous O-mode heating cycle the enhancement is shorter and also in terms of altitude variation not as stable, see Figure 5.12.

The enhancement starts with heater on at 125 km lasting till 17:53:05. For about 12 s starting at 17:52:18 the peak of the enhancement is at an altitude slightly above the previous peak and the enhancement afterwards. The change in altitude is not a continuous change and in Figure 5.20(b) two peaks of enhancement are seen at the same time. At 17 53:40 a short event of enhancement is recorded at an altitude of 125 km.

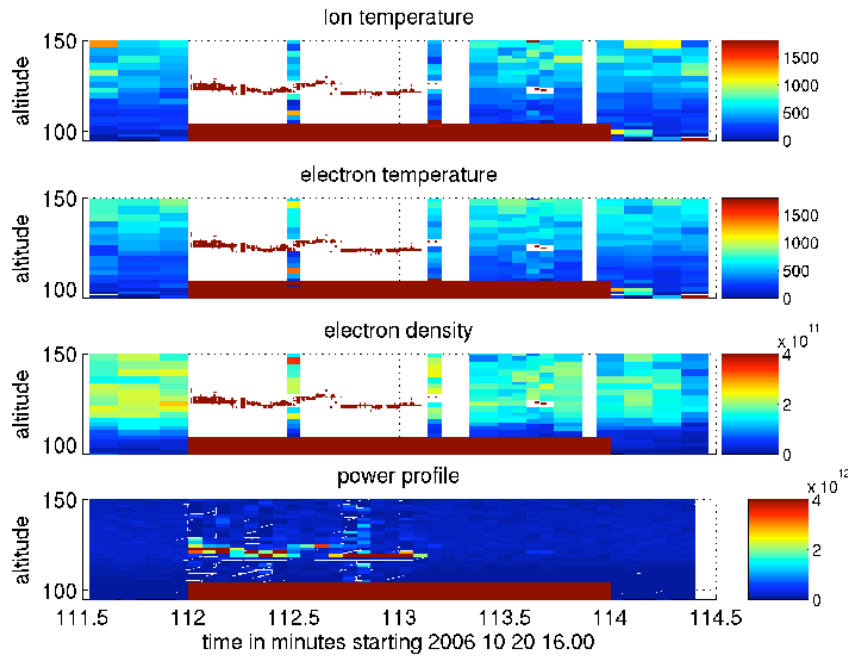
In the region below and close to the enhancement analyzed radar data reveals electron temperatures below 600 K.

Optical data for this heating cycle shows auroral emissions with the ASK1 camera (6730 Å) which is structured on small scales before and in the beginning of the heating cycle. During the heating cycle the auroral emission is getting weaker and returns to background values at the end. ASK2 and ASK3 show only very weak emissions in their covered bandwidth, see Figure 5.16(b).

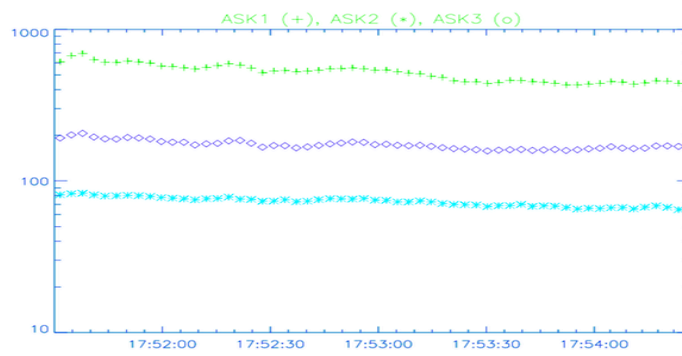
The spectral characteristics of the turbulent region during this heating cycle are shown in Figure 5.17. In Figure 5.18 spectra of two dumps are explicitly shown. Generally spoken the spectra shape of the turbulent regions is of the NR type in the beginning. After 17:52:44 the peaks for the IL are seen but still dominated by the central line. The center frequency of the ILs are below ± 4 kHz for the whole period. The width of the three spectral lines during the times of turbulence is just below 4 kHz as for heating cycle O7.

Power profile: The first of the plots in Figure 5.20 shows strong enhancement with disturbances of the decoded power profile up to 180 km. It also shows the event in chronological order with the turbulence below 120 km and a second peak in enhancement at a higher altitude around 17:52:20, shown in Figure 5.20(b).

Electron density profile: To obtain the density profile it was chosen to average electron density data between 17:50 and 17:52 right after the heating cycle and the observed enhancements in returned power. The profile shown in Figure 5.19 has only one clear peak in the E-region at an altitude of 122 km.



(a)



(b)

Figure 5.16: Same as Figure 5.1 for heating cycle O8.

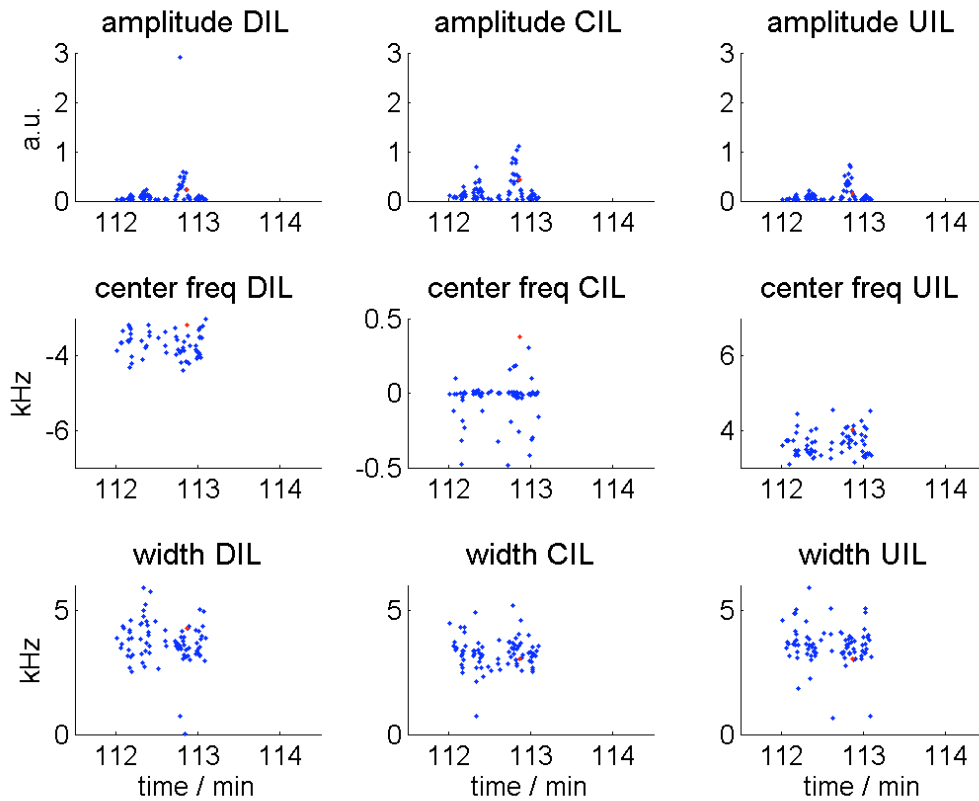


Figure 5.17: Spectra characteristics of enhancements during heating cycle O8, same as Figure 5.2. Although two separated layers are not observed the automated analysis program categorized some of the data points as a separated layer marked red.

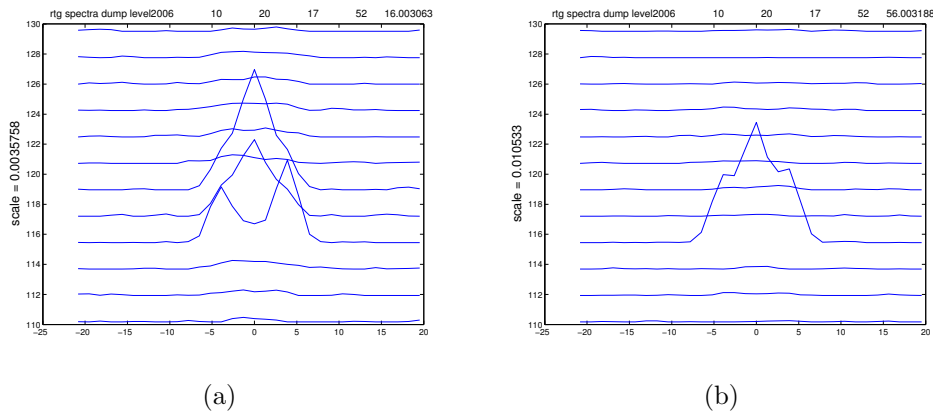


Figure 5.18: Same as Fig. 5.3 for heating cycle O8. a) for the dump ending 17:52:16 and b) for 17:52:56.

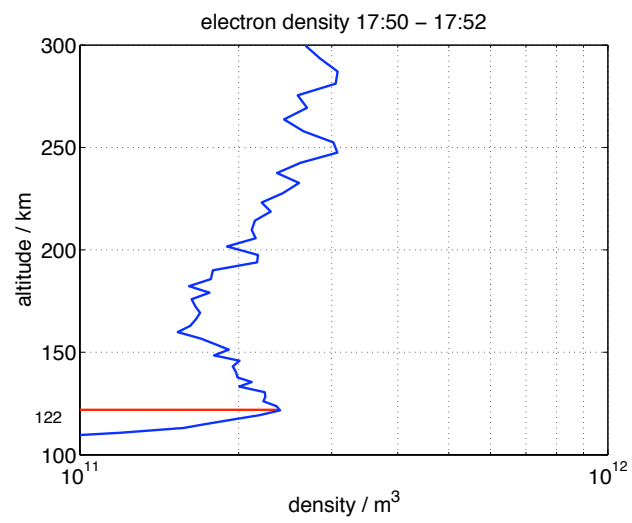


Figure 5.19: Same as Figure 5.4 for the time after heating cycle O8 showing the electron density profile averaged between 17:50 until 17:52. The horizontal red line indicates the local peak in the density profile at 122 km altitude.

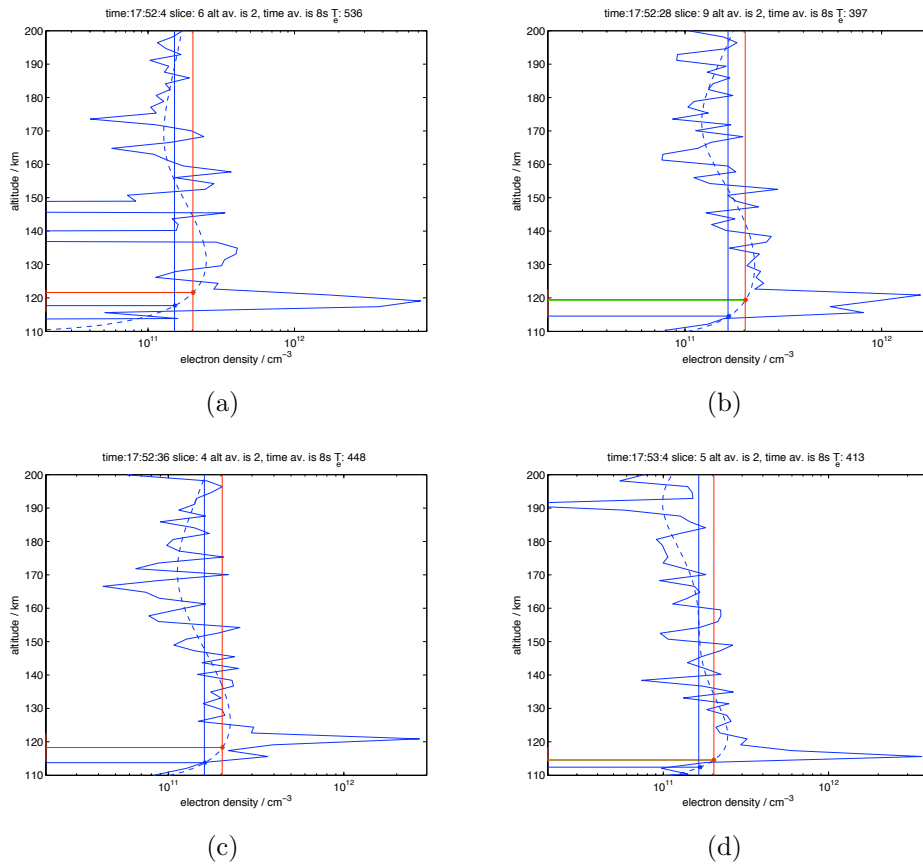


Figure 5.20: Same as Figure 5.5 for heating cycle O8. In the range from 110 to 175 km "decoding noise" is clearly to be seen in Figure 5.20(a). As for heating cycle O7 the modified power profiles shown here have been chosen to have rather less noise.

5.5 Further Analysis

During the evaluation of the analysis done on the spectral characteristics of the triggered instabilities it was observed that the downshifted IL (DIL) was stronger than the upshifted IL (UIL). In Figure 5.21 a histogram plot shows the relative difference in amplitude of the two ILs: $(A_{DIL} - A_{UIL})/A_{DIL}$. Red refers again to turbulent layers rated as top layer and blue to bottom layer. It clearly shows another difference of the top and bottom layer since for both data sets - O1 and O2 - it is only the bottom layer which shows the characteristic of a stronger DIL. The upper layer on the other hand shows a distribution centered at zero.

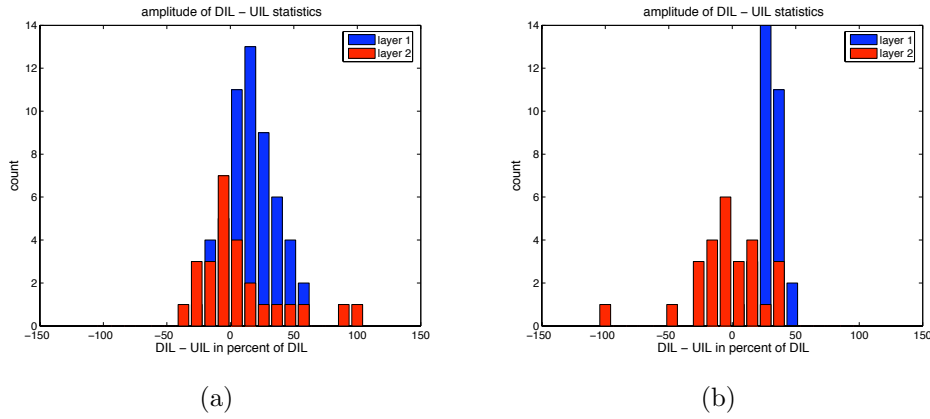


Figure 5.21: Difference in amplitude of DIL and UIL in percentage of the DIL amplitude: $(A_{DIL} - A_{UIL})/A_{DIL}$. a) For heating cycle O1. b) For heating cycle O2.

5.6 Summary of observations

As stated above two altitude separated layers of enhancement were observed during the heating cycles O1 and O2. During the other two discussed heating cycles which are discussed no separation was observed. In order to clarify the observations and ionospheric conditions a summary of the most important issues with respect to the differences between O1-O2 and O7-O8 is given here.

- Heating mode:
During heating cycle O1 and O2 continuous heating was used whereas a 10 Hz on-off modulated heating scheme was used during O7 and O8.

- Electron density profile:
The density profile in the E-region for heating cycle O7 and O8 has a rather parabolic shape with a peak electron density of $\sim 2.2 \cdot 10^{11} \text{ m}^{-3}$ above 120 km.
During O1 and O2 the electron density is close to critical from the bottom to the top of the E-region. Because of the short averaging time for the O1 profile the profile is noise. For O2 however the profile shows two density peaks one at 115 km and the second at 127 km both with a density close to or above critical.
- Electron temperature:
Electron temperature data computed with *guisdap* reveal temperatures of up to 1000 K at altitudes between 100 and 120 km for heating cycle O1 and O2. For the heating cycles O7 and O8 the electron temperature is ~ 500 K.
- Optics:
ASK1 intensity is higher in the beginning of the experiment than later on e.g. ~ 1000 a.u. during O1 and O2, ~ 700 a.u. for O7 and ~ 400 a.u. for O8. The intensities observed with ASK2 and ASK3 are very low in the beginning - approximately 100 a.u. respectively 20 a.u. for O1 and O2 - and rise later to about 200 a.u. and 90 a.u. during O7 and O8. During all four heating cycles structures could be seen in the image data moving from north-east to south-west. No direct link could be found between observed aurora with optics and the observations discussed here except during heating cycle O7. For O7 the intensity of turbulence correlates to the auroral intensities observed with the ASK instrument.
- Spectra:
During the heating cycles O1 and O2 two in altitude separated enhancements were observed. The spectra of this layers are different from each other. The upper layer shows a strong central line and the ion lines with frequencies of about 4 kHz are not resolved. The lower layer shows well resolved ion lines with frequencies of 5 kHz and a strong central line. Another difference between the lower and upper layer is that in the lower layer of enhancement the downshifted ion line is stronger than the upshifted ion line.
For heating cycle O7 also the shape of the spectra seems to correlate to the observed auroral intensities with ASK i.e. the central line is more dominant during increased auroral intensities. Ion lines are resolved during almost the whole time and are centered around 4 kHz up to 5 kHz. During O8 the ILs are only resolved the last 20 s of the enhancement

centered at 4 kHz while during the 40 s in the beginning the central line is dominant.

Chapter 6

Discussion

Ion line spectra in the auroral E-region

The dispersion relationship for the ion acoustic waves - presented in section 3.3 eqn. (3.29) - shows that the ion acoustic frequency is proportional to the square root of the electron temperature. In the ionosphere the electron temperature rises with altitude therefore the ion acoustic frequencies are usually $\sim 4 - 10$ kHz from the bottom to the top. Combined with the fact of high damping at low altitudes the ion acoustic spectra as seen with incoherent scatter radars are usually washed out at low altitudes i.e. the downshifted and upshifted ion line are broad and very close to each other. The spectra presented in chapter 5 which were observed during heating differ to the usually observed ion line spectra in the E-region. Well resolved are the two ion lines and the central peak which was observed during almost all enhancements. The high ion line frequencies specially seen in the lower layer of enhancements during the heating cycles O1 and O2 could imply heating of the electrons during the turbulence.

Dubois et al. [1993] show the altitude allocation of Langmuir turbulence where in the top region close to the reflection altitude a central line is observed and below the reflection altitude enhanced ion lines. This was observed in some of the cases where the turbulence spread over two altitude bins and is seen e.g. in Figure 5.13(b).

Temperature enhancements

During the heating cycles O1 and O2 temperature enhancements at altitudes between 100 and 120 km were observed. Because of increased electron temperatures at this altitude were not only observed during the heating cycles

this enhancement could be caused by auroral processes heating the electrons. However the further enhancement to temperatures of ~ 1000 K during O1 and O2 could be due to absorption of the heater wave at this altitude leading to electron heating.

Correlation of aurora to observed instabilities

During heating cycle O7 correlation between the enhancements and auroral activity is eventual. As seen in the spectral characteristics the increase in returned power during increased auroral activity is mainly due to a stronger central line during such times. This means the shape of the ion line spectra change from the characteristic three lines towards a dominant central line. As stated previously aurora introduces irregularities in the density profile which could favor the OTSI where irregularities and depletions are amplified.

Mode conversion

In the paper by Rietveld et al. [2002] where they observed in a similar experiment enhancements in the ion line from two separated altitudes they argue with E-region topside and bottomside enhancements. The bottomside enhancement occurs due to PDI. Parts of the heater waves energy is converted to a Z-mode wave which then triggers instabilities at the E-region topside - see also Gondarenko et al. [2003].

Electron density profiles computed with EISCAT radar data and presented in section 5 for heating cycle O1 and O2 do not suggest this explanation of the two separated layers for this experiment. According to these it is more likely that the two layers originate from two local and narrow density peaks in the E-region. However the difference in the spectra on the other hand indicate different processes for the two layers. Also the presence of irregularities in the density profile favors the mode conversion which happens usually in a region around the Spitze region. In the case of a smooth profile this region would be out of the region detected with the radar since the UHF radar was used in field aligned position. With this explanation it remains unclear why at times only the topside enhancements are seen.

Comments on PDI

In the presentation of analysis done on data for heating cycles O1, O2, O7 and O8 - see section 5 - the plots of the modified power profiles contain an approximation for the matching height. Although this approximation coincides in many cases pretty well with the lower layer theory does not predict

such observations. The matching height refers to the height where the induced Langmuir waves match a k-vector of twice the radar k-vector. Therefore the induced Langmuir waves rise the measured backscattered radar power at this height - see section 3.4, DuBois et al. [1990], Kohl et al. [1993]. To the authors understanding of of PDI and associated turbulence ion line data with two separate layers is not included in the theory.

Chapter 7

Conclusions

The aim of the heating experiment carried out in October 2006 during auroral conditions was to trigger flickering aurora (see Whiter et al. [2008]) which was not achieved. This report is concentrated on instabilities in the auroral E-region triggered by the heater wave. Such instabilities as seen in the enhanced backscattered radar power of the incoherent scatter radar were found at altitudes of ~ 120 km and at altitudes ~ 150 km close to the reflection altitude of the heater wave. The enhancements in the lower part of the E-region were analyzed in more detail as presented in chapter 5.

During two cycles with 2 min of continuous heating simultaneous enhancements at two altitudes with a separation of about 5 km were observed. The observed ion line spectra imply different processes for the two layers since the upper layer is dominated by a central line ($\omega = 0$) and the lower layer by equally enhanced ion acoustic and central lines.

Rietveld et al. [2002] also observed two layers of enhancement in the E-region in a similar experiment. They argue that the lower enhancement is caused by the heater wave triggering PDI. Whereas the upper enhancement is due to mode conversion of parts of the heater wave to a Z-mode wave triggering instabilities at the topside of the E-layer (see also Gondarenko et al. [2003]). The radar program used for the experiment underlying this report has a fairly low altitude and time resolution in order to observe and characterize instabilities. Also it is a coded program which leads to the problem that during strong enhancements the radar data is noisy. In order to make statements about the density during enhancements modified power profiles (see section 5.1) were made. Although the accuracy of these density profiles has to be questioned they reveal enhancements at the reflection altitude and ~ 5 km below.

During one heating cycle of 2 min 10 Hz modulated O-mode heating enhancements were observed during the whole period (with short interruptions). The comparison of the strength of the enhancements and spectral characteristics

reveal a correlation to auroral intensities measured with the ASK instrument. In the manner of a more dominant central line during times of high auroral emissions.

Bibliography

- Anderson, D. and Fuller-Rowell, T. (2010). <http://de.wikipedia.org/wiki/Datei:IonosphereProfileNOAA.png>.
- Dahlgren, H., Ivchenko, N., Sullivan, J., Lanchester, B. J., Marklund, G., and Whiter, D. (2008). Morphology and dynamics of aurora at fine scale: First results from the ask instrument. volume 26, pages 1041–1048. 32nd Annual Meeting on Atmospheric Studies by Optical Methods, Copernicus Publ.
- Dhillon, R. S., Robinson, T. R., and Yeoman, T. K. (2007). Eiscat svalbard radar observations of spear-induced e- and f-region spectral enhancements in the polar cap ionosphere. *An. Geophys.*, 25:1801–1814.
- Djuth, F. (1984). Hf-enhanced plasma lines in the lower ionosphere. *Radio Sci.*, 19(1):383–394.
- Djuth, F. T., Isham, B., Rietveld, M. T., Hagfors, T., and La Hoz, C. (2004). First 100 ms of hf modification at tromso, norway. *J. Geophys. Res.*, 109(A11307).
- Djuth, F. T., Sulzer, M. P., and Elder, J. H. (1990). High resolution observations of hf-induced plasma waves in the ionosphere. *Geophys. Res. Lett.*, 17(11):1893–1896.
- Dubois, D., Hanssen, A., Rose, H., and Russell, D. (1993). Space and time distribution of hf excited langmuir turbulence in the ionosphere: Comparison of theory and experiment. *J. Geophys. Res.*
- DuBois, D., Rose, H., and Russell, D. (1990). Excitation of strong langmuir turbulence in plasmas near critical density: Application to hf heating of the ionosphere. *J. Geophys. Res.*, 95(A12):21221–21272.
- Duncan, L. M. and Gordon, W. E. (1982). Ionospheric modification by high-power radio-waves. *J. Atmosph. Terr. Phys.*, 44(12):1009–1017.
- Fälthammar, C. G. (2001). Space physics. Book used at KTH for teaching.

- Fejer, J. A. (1979). Ionospheric modification and parametric instabilities. *Rev. Geophys.*, 17(1):135–153.
- Gondarenko, N. A., Guzdar, P. N., Ossakow, S. L., and Bernhardt, P. A. (2003). Linear mode conversion in inhomogeneous magnetized plasmas during ionospheric modification by hf radio waves. *J. Geophys. Res.*, 108(A12).
- Gurnett, D. A. and Bhattacharjee, A. (2005). *Introduction to Plasma Physics, With Space and Laboratory Applications*. Cambridge University Press.
- IRI (2010). <http://www.omniweb.gsfc.nasa.gov/vitmo/iri-vitmo.html>.
- Isham, B., La Hoz, C., Rietveld, M. T., Hagfors, T., and Leyser, T. B. (1999a). Cavitating langmuir turbulence observed during high-latitude ionospheric wave interaction experiments. *Phys. Rev. Lett.*, 83(13).
- Isham, B., Rietveld, M. T., Hagfors, T., La Hoz, C., Mishin, E., Kofman, W., Leyser, T. B., and van Eyken, A. P. (1999b). Aspect angle dependance of hf enhanced incoherent backscatter. *Adv. Space Res.*, 24(8):1003–1006.
- Kohl, H., Kopka, H., Stubbe, P., and Rietveld, M. (1993). Introduction to ionospheric heating experiments at tromso. 2. scientific problems. *J. Atmosph. and Terrest. Ph.*, 55:601–613.
- Kuo, S. P. (2001). Cascade of parametric instabilities in ionospheric heating experiments. *J. Plasma Phys.*, 66(5):315–336.
- Kuo, S. P. (2002). Oscillating two-stream instability in ionospheric heating experiments. *Phys. Plasmas*, 9(4):1456–1459.
- Kuo, S. P. (2003). On parametric instabilities in hf heating of the ionosphere. *J. Plasma Phys.*, 69(6):529–540.
- Lehtinen, M. S., Huuskonen, A., and Pirttila, J. (1996). First experiences of full-profile analysis with guisdap. volume 14, pages 1487–1495. VIIth EISCAT workshop, Springer Verlag.
- Leyser, T. B. and Nordblad, E. (2009). Self-focussed radio frequency l wave pumping of localized upper hybrid oscillations in high-latitude ionospheric plasma. *Geo. Res. Let.*, 36(L24105).
- Leyser, T. B. and Wong, A. Y. (2009). Powerful electromagnetic waves for active environmental research in geospace. *Rev. Geophys.*, 47.
- Loefas (2008). Ionospheric modification by powerful hf-waves, underdense f-region heating by x-mode.

- Lundborg, B. and Thide, B. (1986). Standing wave pattern of hf radio waves in the ionospheric reflection region 2. applications. *Radio Sci.*, 21(3):486–500.
- MSIS (2010). <http://ccmc.gsfc.nasa.gov/modelweb/models/msis-vitmo.php>.
- Paschmann, G., Haaland, S., and Treumann, R. (2003). *Auroral Plasma Physics*. Space Science Series of ISSI. Kluwer Academic Publishers.
- Rietveld, M., Isham, B., Kohl, H., La Hoz, C., and Hagfors, T. (2000). Measurements of hf-enhanced plasma and ion lines at eiscat with high-altitude resolution. *J. Geophys. Res.*, 105(A4):7429–7439.
- Rietveld, M., Kohl, H., Kopka, H., and Stubbe, P. (1993). Introduction to ionospheric heating at tromso. 1. experimental overview. In *J. Atmosph. Terr. Phys.*, volume 55, pages 577–599. European Incoherent scattering Sci Assoc, Pergamon-Elsevier Science Ltd.
- Rietveld, M. T. (2010). <http://www.eiscat.uit.no/heater.html>.
- Rietveld, M. T., Isham, B., Grydeland, T., La Hoz, C., Leyser, T. B., Honary, F., Ueda, H., Kosch, M., and Hagfors, T. (2002). Hf-pump-induced parametric instabilities in the auroral e-region. In Raitt, W. J. and Shukla, P. K., editors, *Advances in Space Research*, volume 29, pages 1363–1368. COSPAR, Pergamon-Elsevier Science Ltd.
- Shoucri, M. M., Morales, G. J., and Maggs, J. E. (1984). Ohmic heating of the polar f region by hf pulses. *J. Geophys. Res.*, 89(A5):2907–2917.
- Stubbe, P., Kohl, H., and Rietveld, M. (1992). Langmuir turbulence and ionospheric modification. *J. Geophys. Res.*, 97:6285–6297.
- TimeandDateAS (2010). <http://www.timeanddate.com/worldclock/astronomy.html?n=290&month=10&year=2006&obj=sun&afl=-11&day=1>.
- Whiter, D. K., Lanchester, B. S., Gustavsson, B., Ivchenko, N., Sullivan, J. M., and Dahlgren, H. (2008). Small-scale structures in flickering aurora. *Geoph. Res. Let.*, 35(23).